NASA

MEMORANDUM

EXPLORATORY STUDY OF VENTILATED FLOWS ABOUT

YAWED SURFACE-PIERCING STRUTS

By John P. Breslin and Richard Skalak

Experimental Towing Tank
Stevens Institute of Technology

NATIONAL AERONAUTICS AND SPACE ADMINISTRATION

WASHINGTON

April 1959

NATIONAL AERONAUTICS AND SPACE ADMINISTRATION

MEMORANDUM 2-23-59W

EXPLORATORY STUDY OF VENTILATED FLOWS ABOUT

YAWED SURFACE-PIERCING STRUTS

By John P. Breslin and Richard Skalak

SUMMARY

Reported herein are the results of observations and measurements
made in connection with a study of the phenomenon of the development of
atmosphere-connected cavities about surface-piercing struts. Conditions
for the existence of such ventilated flows which have been derived from
the experimental data are presented. In addition, certain broad con-
clusions pertinent to model testing and full-scale design are reached.
Further experimentation to define the inception of ventilation as a
function of boundary-layer state or Reynolds number is required.

INTRODUCTION

The present report is an account of an exploratory study of flow
ventilation about surface-piercing foils. By ventilation is meant the
occurrence of atmosphere-connected cavities usually on one side and abaft
a moving, surface-piercing body. This phenomenon is to be distinguished
from cavitation in which pressure in the cavity is equal to the vapor
pressure of the fluid at the local temperature. However, for the sake
of brevity, the term "cavity" will often be used in the following pages
in lieu of the more cumbersome term "ventilated cavity." References
to vapor cavities will be specifically designated as such.

This report was motivated by the need to know the mechanism by
which these atmosphere-fed cavities are incepted and the conditions
under which this flow pattern can exist. This need originated during
development testing of seaplanes and hydrofoil-boat foils which showed
peculiar results when tested with ventilation at different scales.

The study was carried out using two foils of widely different sec-
tions which were towed as vertical surface-piercing struts. Close
observations of the flow patterns were made and are reported herein.
Several forms of ventilation inception are described, and the behavior
of the side force and drag is delineated. Boundary-layer observations

were made in a manner recently developed by the Hydrodynamics Division
at the Langley Aeronautical Laboratory of the National Advisory Committee
for Aeronautics. General criteria for the existence of ventilation are
set down and conclusions applicable to model testing and full-scale
design are given.

The present investigation was conducted at the Experimental Towing
Tank, Stevens Institute of Technology under the sponsorship and with
the financial assistance of the NACA.

SYMBOLS

A	aspect ratio
A_1, A_2, A_3	coefficients in equations (11) and (12)
C_D	drag coefficient
C_L	lift coefficient
C_S	side-force coefficient
c	strut chord
D	drag
F	Froude number
F_h	submergence Froude number
f	camber ratio
g	acceleration due to gravity
h	submerged length of foil in calm water
p	pressure at any point in fluid
p_v	vapor pressure of water
p_∞	pressure far upstream of disturbance
R	chord Reynolds number

S	side force
t	strut thickness
U	free-stream velocity or speed of advance
u,v,w	x, y, and z components of perturbation velocity
V	resultant velocity
x,y,z	Cartesian coordinates
α	angle of attack or yaw, deg
γ	half of central angle subtended by circular-arc section, deg
ζ	surface deformation
ρ	mass density of water
σ	cavitation index
ψ	yaw angle of strut

DESCRIPTION OF EXPERIMENTS

Experiments were performed on two vertical struts, one having an NACA 4412 airfoil section with a 3-inch chord and the other having a symmetrical circular-arc section with a maximum thickness of 0.306 inch and a 2.50-inch chord.

Both struts were tested in vertical positions only, at aspect ratios of 0.5, 1.0, 1.5, and 2.0 over a range of angles of attack or, more properly, of yaw. The aspect ratio was defined simply as the calm-water submerged length divided by the chord length inasmuch as both foils were of rectangular plan form.

The NACA 4412 foil also was tested with an end plate 8 inches in diameter and 1/16 inch thick attached to the lower end and parallel to the still water surface.

The struts were towed at a radius of 31 feet on the rotating arm in Tank 2 at the Experimental Towing Tank, Stevens Institute of Technology. This facility was employed because it is possible for an observer to ride the rotating arm, and thereby precisely to control the experiment as well

as to note the changing flow pattern. A view of the test arrangement is shown in figure 1.

Side-force and drag curves were determined in all cases except for the NACA 4412 foil with an end plate. Two additional curves of the velocities and angles of yaw at inception and closure of ventilated cavities were determined in each case. First, by gradually increasing the velocity at a fixed aspect ratio and angle of yaw, the minimum velocity at which a cavity formed spontaneously was observed. Second, by holding the yaw angle fixed and gradually decreasing the velocity after a cavity had formed, the velocity at which the cavity closed was recorded. A maximum velocity of 30 feet per second did not cause a cavity to form spontaneously in all cases of angle of yaw below 19^C for the NACA strut and below 13° for the circular-arc strut. In these cases a cavity was initiated by causing a disturbance just ahead of the foil or along its suction side. A corner of a 3-foot wood rule or a 1/4-inch steel rod was used to create the disturbance. A comparatively small disturbance at the surface initiated a cavity if the speed was substantially above those low speeds at which the cavity closed when left undisturbed. In addition, a cavity was initiated easily by such a disturbance when the speed was considerably less than that required to produce a cavity spontaneously. Thus, for a given angle of attack a speed range was determined for which two flow regimes were found possible, namely, one in which the suction side remained wetted and another in which the suction side was completely connected to the atmosphere or ventilated.

Boundary-layer flow studies were conducted to show a correlation between inception and boundary-layer separation. These tests are described later in this report.

FLOW PATTERNS AND MODES OF VENTILATION INCEPTION

Spontaneous Inception

Two principal types of spontaneous (or self-generated) inception were observed. One type attended the transient motion of the separated flow region, and the other type took place through aeration of the trailing tip vortex which drew air to the bottom tip of the foil.

The former type is most easily observed at very large angles of attack (or yaw), of the order of 30° for the foils tested. For this range of angles a clearly defined "dead" wake can be detected behind the foils. This turbulent wake, which is similar to the wake behind any blunt body, is depressed slightly at low speeds of 1 or 2 feet per second. This depression is readily understood in terms of the notion of

base pressure (or pressure on the stern) in two-dimensional flow around a blunt body in an infinite fluid. Base pressure is negative with respect to the reference pressure at infinity. Hence, on the surface-piercing strut the negative pressure below the free surface and the low velocity of the wake fluid accounts for the drop in the water level immediately abaft the strut.

As the velocity increased, the depth of the depression increased. The partial cavity filled with "bubbly" fluid which appeared to be the result of water tumbling from the sides and rear of the cavity into the deepest part of the cavity as indicated in figure 2. When the velocity was sufficiently high, the frothy water swept back and a smooth-walled cavity was formed by solid walls of water streaming backward from the outer edges of the bottom of the foil. A general outline of this pattern is given in figure 3. The transition from a froth-filled region to a cavity with smooth walls occurred at a distinct velocity. This velocity was recorded as a minimum necessary to form a cavity.

The gradual formation of a cavity at large yaw angles also takes place when a surface-piercing flat plate is held at right angles to the direction of motion. The above-described sequence of events also can be applied to blunt bodies (cylinders, wedges, or rectangular bars with either long or short sides parallel to the velocity vector) which pierce a fluid surface.

The formation of a full-depth, air-connected or open cavity by a gradual depression of a dead wake appears to take place at a constant velocity and independent of the yaw for each foil and aspect ratio. This was true for the small range of large angles tested. As the angle of yaw is decreased, a point is reached at which the formation of the cavity is no longer gradual. Instead the cavity suddenly opens fully. This occurs at a certain velocity which is higher for small than that for large angles of yaw.

Spontaneous ventilation occurs for a range of 4° or 5° starting from an angle of 15° to 18° for the circular foil. The range for the NACA foil is smaller, being about 2° or 3° and occurring at larger angles, between 22° to 26°. The exact range depends on the aspect ratio.

The sudden-separation ventilation is usually so rapid that one could see only the initial and final states. It is accompanied by a distinctive gurgling sound similar to the noise caused by air being drawn into a vortex formed above a drain in the bottom of a shallow open tank. When the velocity is relatively low, say 6 to 8 feet per second, the inception mechanism may make several attempts before a cavity is formed. During these attempts the gurgling noise is heard and air bubbles are

6

seen circulating about a vertical axis in a region adjacent to the suction side of the foil as indicated in figure 4. After an unsuccessful attempt at initiating ventilation these bubbles are swept downstream.

Motion pictures were taken of the NACA 4412 foil in order to see clearly how this mode of aeration took place [1] These pictures show that the process begins with the development of an unsteady swirling motion in the immediate vicinity of the trailing edge. This unsteadiness is caused by the shifting of the front of the separation region of the boundary-layer flow toward the leading edge after the angle of yaw is increased slightly. The swirling wake quickly develops a "momentary" Rankine free-surface vortex which provides a passage allowing a quantity of air to enter the separated zone. This ingestion or "swallowing" is heard as a gurgling noise. The air in the separated zone moves about as bubbles which flow toward the front of the separation. The attached flow at large angles (22° to 26° for the NACA 4412 foil) develops very large pressure drops which provide a large gradient on the bubbles which float close to the separation front.

The final stage in the development of the completely aerated cavity flow is believed to be generated by the sudden expansion of one or more of these air bubbles as they come near the very low pressure, attached flow region. This expansion ruptures the free surface just abaft the leading edge with the result that a completely new stream surface develops clear of the suction side. This transition takes place so quickly that the camera speed of 128 frames per second was not high enough to resolve the motion. Hence, the description of this last phase is somewhat conjectural. The mechanism of the first phase is well established, particularly in view of observed "unsuccessful attempts" in which air bubbles circulate about and do not expand before they are caught and swept away by the main stream. A schematic drawing of the pattern with ingested air bubbles is given in figure 4.

Both the steady, progressive ventilation and the sudden ventilation at somewhat smaller angles attend the development of boundary-layer separation, which is, of course, a function of Reynolds number (except in the case of forms with sharp edges). Thus, this type of inception can be associated with those side-force coefficients at stall. The occurrence of stall is the gross or integrated manifestation of boundary-layer separation.

---

[1] A motion-picture film supplement has been prepared and is available on loan. A request card form and a description of the film will be found at the back of this paper, on the page immediately preceding the abstract and index pages.

The second principal type of spontaneous cavity is due to aeration of the tip vortex which trails the foil from the submerged tip. This type of ventilation was observed on the NACA 4412 foil at aspect ratios of 1.5, 1.0, and 0.5 and for the circular-arc foil only at an aspect ratio of 0.5. Tip-vortex ventilation occurred only at fairly large angles in a range of 4° or 5° located somewhere between 13° and 29° for the various cases tested. At smaller angles the maximum test speed of 30 feet per second was insufficient to produce an aerated vortex core. Hence, a complete set of conditions at which this mechanism provided ventilation was not determined.

The flow patterns just prior to ventilation via the tip vortex are shown in figure 5. In the most typical flow pattern (fig. 5(a)) the center of the tip vortex is filled with air, forms a tube which trails behind the foil, and comes to the surface at a distance some 20 chord lengths or more downstream. This distance depends on speed, aspect ratio, and angle of yaw. The tube appeared to be parallel to the surface just behind the foil and to intersect the free surface at a small angle. (The point of intersection was not clear because the spray and foaming of the wake obscured it.) Aeration of the vortex center occurred from the rear. The tip of the aerated portion moved forward as the velocity increased. When it reached the strut, a full cavity usually formed with a loud, sharp report. Sometimes the aerated vortex clung to the lower tip of the foil and the cavity did not form until the velocity was raised slightly. A gurgling, sucking noise accompanied the aeration of the tip vortex. Photographs of this flow phenomenon are given in figure 6.

At the aspect ratio of 0.5 another form of aerated vortex was observed as shown in figure 5(b). In this case the tip vortex first ventilated as described above, then grew in diameter and assumed a cigar shape as shown in the sketch with the leading end being about 1/2 inch behind the trailing edge of the foil. This balloon shape persisted in some cases for a considerable range of velocity before a cavity was finally formed. Similar aerated vortices, observed in the wakes of low-aspect-ratio plates, are described in reference 1.

Forced Inception and Other Possible Mechanisms

It was noted that, for a wide range of angles, ventilated cavities could be produced by a disturbance but could not form spontaneously. The flow was unstable with regard to disturbances initiated in the neighborhood of the leading edge but stable with regard to similar disturbances in the vicinity of the trailing edge. The disturbances were made by lightly inserting the head of a pencil or the corner of a wood ruler into the juncture of the free surface and the strut. A momentary flow separation took place immediately abaft of the disturbing element,

while at the same time the sealing action of the thin layer of fluid which formed the "spray sheet" on the suction side was disrupted. Most such perturbations of the flow near the leading edge produced an inception of the ventilation at the trailing edge. The ventilated region then instantly moved forward to its equilibrium position. The location of the front of the ventilated region was observed to be somewhat removed from the leading edge of the NACA strut, whereas the ventilation on the circular-arc strut moved immediately to the sharp leading edge.

At this point it is of interest to note the existence of other mechanisms by which ventilation can be induced. One possible type of inception which was not observed in the tests is through aeration of the cores of the vertical vortices when the strut leaves a Karman vortex street behind it. This is most likely to occur in the case of struts with blunt trailing edges. The inception of ventilation through vertical vortices of the vortex street is shown clearly in photographs given by Gongwer in reference 2. In Gongwer's case the foil was a diamond or double-wedge shape with a 12-inch chord and a trailing-edge thickness of 1/8 inch. The experiments were at 32 knots and had an espect ratio of 1. Additional examples may be found in photographs presented by Kaplan in reference 3 and by Hay in reference 4.

A second possibility for ventilation inception at high velocities is through the formation of a cavitating region at vapor pressure at some point on the strut below the surface. Cf course, cavitation without ventilation is possible on a surface-piercing body as observed by Coffee and McKann in reference 5. They detected a cavitation region at about middraft on a surface-piercing strut at zero yaw. (An improved method of predicting the inception speed and location in such cases has been developed by Breslin in ref. 6.) However, it is conceivable that such vapor cavities may grow with further increase of speed (beyond that for inception) until the air pressure above the fluid is able to implode the layer of water separating the free surface from the cavity at vapor pressure. It is expected that this occurrence would be accompanied by a loud, sharp report.

To postpone the inception of ventilation of surface-piercing bodies which develop lift or side force, it appears advisable to reduce the local side loading near the juncture with the free surface so that the generation of regions of boundary-layer separation will be avoided. This can be done by increasing the chord and, in the case of dihedral foils, by reducing the angle of attack through twist.

Wake Forms

Various patterns of spray sheets and other wake characteristics observed fall into a few more or less distinct categories. Figure 7

shows a typical condition when ventilation is not present. A thin spray sheet is always thrown upward and aft from the pressure side of the foil. The absence of a similar spray sheet on the suction side is a "trade mark" of the unventilated condition (see fig. 1). The waterline along the suction side drops and clings smoothly to the foil. At the trailing edge of the suction side and pressure side, flows coalesce at vectorially different velocities and the result is a peculiar "cave" as shown in section AA of figure 7. The upper half of the cave wall develops into a surface-vortex spray as the flow moves downstream (see section BB in fig. 7). Another surface spray caused by the tip vortex coming near the surface could develop still further downstream. This is shown in section CC of figure 7. At low speeds neither the surface-vortex spray nor the tip-vortex spray develops, but the surface becomes undulated or turbulent without breaking into spray at these places.

In all wake forms high and low speeds are relative. Generally, the lower the angle of attack and the aspect ratio, the higher will be the speed required to reach what are called herein high-speed forms. Also, as the speed increases, both the height and length of the forms described increase. At low angles of attack the forms are comparatively low in height and elongated horizontally.

Different center-roach positions allow classification of the wake forms with a cavity into three types. A high-speed form exists over most of the range in which cavities are possible. This is shown in figure 8. The distinguishing feature of this form is that the top surface of the center roach shifts from the suction side toward the pressure side as it moves downstream. In so doing it often traps a cigar-shaped pocket of air and makes a distinctive "hollow pipe" noise. A subsurface view of a completely ventilated cavity is shown in figure 9(a) and a rear view is shown in figure 9(b).

Upon reducing the speed, the center roach gradually loses it rotational motion. Over a small range of speeds it moves straight up and back, spilling more or less symmetrically to both sides. A typical wake form with a cavity at medium speeds is shown in figure 10. The walls and bottom of this cavity are smooth. Distinct vertical spray sheets are thrown up from both suction and pressure sides of the foil. The spray sheet from the suction side is lower and thinner, but both sheets are relatively thin compared with the lower center roach. The center roach is a smooth continuation of the rising bottom of the cavity and is a heavy jet compared with the spray sheets.

In opposition to the high-speed condition, at low speeds just before closure of the cavity the center roach leans toward the suction side. Another typical feature of the low-speed condition is the trailing, aerated tip vortex as shown in figure 11. The air supply for this vortex is obtained through the main cavity to which it was attached. This aerated vortex trails behind the foil to 50 or 60 chord lengths before finally breaking up into segments and discrete air bubbles which rise to the surface.

An interesting sequence of events took place when the speed of a foil with a trailing aerated vortex such as that shown in figure 11 was gradually increased. The point at which the bubbles of air in the trailing vortex reached the surface moved toward the foil as the speed was increased. This behavior was opposite to the general rule that the wake forms elongate in plan view with increasing speed. The explanation appears to be that the free surface affects the tip vortex in a way similar to a rigid wall when the Froude number is very low but behaves more like a true constant pressure surface when the Froude number is high.

Effects of End Plate

The NACA foil was tested with a circular end plate 8 inches in diameter and 1/16 inch thick fastened to the lower end of the strut so that the plate was parallel to the surface and perpendicular to the foil. This arrangement was tested at an aspect ratio of 1, the depth and chord each being 3 inches. The velocity at which a cavity opened spontaneously and the speed at which the cavity closed was determined. The different wake forms shown in figures 7, 8, 10, and 11 again were observed except that in no case was an aerated tip vortex evident either at medium speed or at low speed.

The only type of ventilation observed with the end plate in place was the separation type. The absence of the tip vortex is explained qualitatively by the fact that the plate tends to produce conditions similar to those for an infinite foil. In the infinite case the vorticity vector remains parallel to the strut and does not turn downstream as it does at the tip of a finite foil to form the trailing vortex. Using an end plate, the lifting vortex may be imagined to terminate on the plate, which is permissible in the sense that vortex lines must end on a boundary or form closed loops. Perhaps a more practical explanation is that the end plate blocks the passage of fluid from the pressure to the suction side over the tip, thus preventing the generation of a vortical flow.

The practical conclusion here implies that a tip-vortex type of spontaneous ventilation inception is unlikely when a strut or foil is terminated by a plane surface perpendicular to the foil. This mechanism could be important in the case of ventral foils.

RESULTS AND DISCUSSION OF SIDE-FORCE MEASUREMENTS

Side-Force Variation for Strut of NACA 4412 Foil

The uppermost curves on figure 12(a) through 12(c) show the side-force coefficients for the NACA 4412 foil when run as a surface-piercing strut at aspect ratios of 0.5, 1.0, 1.5, and 2.0 without ventilation. Curves showing the coefficients pertaining to flows with cavities present at the various Froude numbers indicated are also presented.

The typical features of these curves are best exhibited in figure 12(b) at an aspect ratio of 1 for which more extensive data were taken. Regarding the uppermost curve of coefficients for flows without a cavity, it is notable that Froude number effects are absent in the range of $2 \leqq F = (V/\sqrt{gc}) \leqq 6$ for which points are shown. The points for $F = 2, 4,$ and 6 all lie on the same line. However, in the cases where cavities formed, distinct curves result for $F = 2, 4,$ and 6 as shown. The curves for $F = 4$ and $F = 6$ are closer for large angles than for small angles and approach the closure point for the $F = 4$ case. For $F = 6$ and $F = 8$ the curves are the same (within experimental error) which indicates that variation with the Froude number is limited to the range below $F = 6$ when cavities are present.

The broken lines with arrows pointing downward, which are shown on the right-hand side of these figures, indicate the angles at which cavities would open spontaneously at the Froude numbers indicated for each line. These angles were determined from separate tests which will be described later. The broken line is used to indicate that no intermediate points along it can be achieved in a steady state since the cavity opens suddenly and fully in these cases.

A vertical line indicating a cavity opening was not evident when $F = 2$ because the velocity was too low to produce a spontaneous cavity in the range of angles tested. It was possible, however, to obtain cavities at $F = 2$ by creating a disturbance at the leading edge of the foil as previously described. The curve marked $F = 2$ shows the coefficients obtained for variable angles down to the angle at which the cavity closed. This curve is smooth, corresponding to the fact that the cavity closed gradually at this Froude number.

The vertical broken lines for $F = 4$, shown on the left side of figures 12(b) and 12(c), indicate the angles at which a cavity at $F = 4$ closes. These angles also were determined from tests which will be discussed later. The broken line is used to indicate that the closure is sudden and no intermediate points can be obtained in a steady-state condition. Vertical lines for cavity closures at $F = 6$ and $F = 8$ are not shown because there were no angles at which a cavity would close within the range tested.

The uppermost and lowest curves of figure 12(b) form the boundaries of a region which contains all possible curves for an aspect ratio of 1. For aspect ratios of 0.5 and 1.5, only a few points defining the bounding curves were determined (see fig. 12(a)). More extensive data for an aspect ratio of 2 are shown in figure 12(c). A peculiarity of this figure is found at high angles for $F = 2$ where the side-force coefficient appears to have a maximum at about $25°$ with a cavity open. The occurrence of a maximum at an angle below $45°$ may be expected from the behavior of fully cavitating cambered foils as predicted by the nonlinear theory shown in figure 5 of reference 7.

Side-Force Variation for Strut of Circular-Arc Foil

Figures 12(d) through 12(f) show the side-force coefficients developed by the circular-arc strut for aspect ratios of 0.5, 1, 1.5, and 2. Figure 12(f), for an aspect ratio of 2, gives the most complete data. All features discussed in the preceding section with respect to the strut of the NACA 4412 foil also may be observed in figure 12(f). Again it is evident that Froude number effects are present up to $F = 6$ when a cavity is open. A variation of the force coefficients also was observed for cases up to $F = 6$ when a cavity was absent. The three uppermost curves in figure 12(f) for $F = 2$, 4, and 6 all are for no cavity or the completely wetted condition. The peculiar "jog" in the curve is due to the fact that the sharp leading edge causes a separation of the flow at the leading edge with a subsequent reattachment. Thus, the effective camber of the foil changes with Reynolds number. The different shapes of these force curves are due entirely to the Reynolds number variation rather than to the Froude number changes inasmuch as the separation phenomena are a function of the Reynolds numbers. This will be discussed again later.

For aspect ratios of 0.5, 1, and 1.5 only the limiting curves of the side coefficients at high Froude numbers were determined for two conditions with and without a cavity present in each case. The results are shown in figures 12(d) and 12(e).

At a Froude number of 2 in figure 12(f), a velocity of 5.18 feet per second is not sufficient to cause a cavity to form. However, as the angle of attack is decreased after a cavity is formed by a disturbance, the cavity closes gradually as is also displayed for the NACA foil for $F = 2.0$ in figure 12(b). Side forces for attached flows at yaw angles in excess of $20°$ were not measured at $A = 2$ and hence no open spots are shown for this region in figure 12(f).

Comparison of Force Coefficients For Fully Ventilated

Strut and Completely Cavitated Hydrofoil Section

It is of interest to attempt a comparison between a fully ventilated flow in three dimensions and a fully cavitated flow in two dimensions. For steady flows with a free surface the Bernoulli equation gives

$$g\zeta + \frac{p}{\rho} + \frac{1}{2}\left[\left(u_3 - U\right)^2 + v_3^2 + w_3^2\right] = \frac{p_\infty}{\rho} + \frac{1}{2} U^2 \tag{1}$$

where

$\zeta = \zeta(x,y)$ surface deformation as measured from undisturbed plane $z \equiv 0$

g acceleration due to gravity

u_3, v_3, w_3 x, y, and z components of perturbation velocity (subscript 3 is appended to emphasize that flow is three-dimensional)

p pressure at any point in fluid

p_∞ pressure far upstream from disturbance

U free-stream velocity taken parallel to negative x-axis

For any point on the free surface $p = p_\infty = $ Constant and hence

$$\frac{2g\zeta}{U^2} = \frac{2}{F_\zeta^2} = \frac{2u_3}{U} - \left[\left(\frac{u_3}{U}\right)^2 + \left(\frac{v_3}{U}\right)^2 + \left(\frac{w_3}{U}\right)^2\right] \tag{2}$$

Now consider a two-dimensional, cavitating hydrofoil section. For this case the relationship between pressure and velocity is

$$\frac{p}{\rho} + \frac{1}{2}\left[\left(u_2 - U\right)^2\right] + v_2^2 = \frac{p_\infty}{\rho} + \frac{1}{2} U^2 \tag{3}$$

where the subscript 2 emphasized that the flow is two-dimensional for any point on the cavity $p = p_v$, the vapor pressure, so that

$$\frac{p_\infty - p_v}{\frac{1}{2}\rho U^2} = -2\left(\frac{u_2}{U}\right) + \left(\frac{u_2}{U}\right)^2 + \left(\frac{v_2}{U}\right)^2 = \sigma \qquad (4)$$

where σ is the cavitation index.

Thus, one might expect that the flow pattern of the ventilated flow at some fixed point where $\zeta < 0$ will be similar to that for the cavitating flow at the cavitation number,

$$\sigma = -\frac{2g\zeta}{U^2} = -\frac{2}{F_\zeta^2} \qquad (\zeta < 0) \qquad (5)$$

In order for this similarity to exist, it would appear necessary that the ventilated section at a depth ζ be quite free of three-dimensional effects which enter principally through the term $\left(w_3/U\right)^2$. The magnitude of this term is emphasized by recalling that the linearized kinematic condition on the free surface relates w_3 to the longitudinal slope of the surface by

$$-\frac{w_3}{U} \approx \left(\frac{\partial\zeta}{\partial x}\right) \qquad (6)$$

This slope is appreciable in the immediate vicinity of the bottom of the strut and also at the trailing edge of the ventilated cavity. It is also significant near the free surface although this region (with the exception of the spray sheets) is not curved nearly so much longitudinally as the flow at the bottom of the pocket. Thus, intuitively, one cannot expect to obtain a good correlation between the side force of ventilated struts and the lift coefficient of a cavitating section at the equivalent σ as given by equation (5) unless the aspect ratio is so large that the relieving effects of both the lower end and the free surface play a small part in the total pattern. It is, nevertheless, of interest to find how well one may approximate the side load on a ventilated strut by summing up the contributions of each spanwise strip. This is done by assuming that the local loading is equal to a cavitating section at an effective σ as given by equation (5).

Under this assumption the side-force coefficient of the finite-aspect-ratio strut, approximated by

$$C_s\left(\psi,F_h\right) = \frac{1}{h} \int_{-h}^{0} C_L(\alpha,\sigma)dy \qquad (7)$$

where

$$\sigma(y) = -\frac{2gy}{U^2}$$

$$dy = -\frac{U^2 d\sigma}{2g}$$

and ψ is the yaw angle of the strut, is

$$C_s = \frac{F_h^2}{2} \int_0^{2/F_h^2} C_L(\alpha,\sigma)d\sigma = \overline{C}_L\left(\alpha,\frac{2}{F_h^2}\right) \qquad (\psi \approx \alpha) \qquad (8)$$

In words, equation (8) simply states that the side-force coefficient is equal to the mean value of the lift coefficient of the cavitating section in the interval of cavitation numbers $0 \le \sigma \le 2F_h^{-2}$.

The variation of $C_L(\alpha,\sigma)$ with σ for a flat plate at small and moderate values of α is very complicated as shown by Wu in reference 7. For $\alpha > 60^{\circ}$, the simple form given by

$$C_L(\alpha,\sigma) = C_L(\alpha,0)(1 + \sigma) \qquad (9)$$

is applicable as Wu also has shown. As a first attempt, equation (9) may be inserted in equation (8) and the following result obtained:

$$C_s\left(\psi,F_h\right) = C_L(\alpha,0)\left(1 + \frac{1}{F_h^2}\right) \qquad (10)$$

This is the same form as that obtained by Perry in reference 8 for the drag coefficient of a ventilated bar of large submergence (aspect) ratio. Comparison of this result with data obtained from the fully ventilated

NACA 4412 section foil at an aspect ratio of 2 is shown in figure 13. (The use of the flat-plate cavitation theory for comparison with this section is justified on the basis that the pressure side of the 4412 section is nearly flat.) It is seen that neither the magnitude nor the character of the Froude number dependence is exhibited by this approximation which is too gross for an angle of attack of 20°.

Since the variation of the lift of a cavitating section with σ for small and moderate α is strongly nonlinear, equation (9) is replaced by the following interpolation formula

$$C_L(\alpha,\sigma) = C_L(\alpha,0)\left[1 + A_1(\alpha)_\sigma + A_2(\alpha)_\sigma^2 + A_3(\alpha)_\sigma^3\right] \qquad (11)$$

where A_1, A_2, and A_3 can be found by fitting this function to the curves given in figure 9 of reference 6 for various α's as a function of σ for a fully cavitating flat-plate section. Then equation (10) is replaced by

$$C_s\left(\psi,F_h\right) = C_L(\alpha,0)\left(1 + \frac{A_1}{F_h^2} + \frac{1.A_2}{5\,F_h^4} + \frac{2A_3}{F_h^6}\right) \qquad (12)$$

Values of coefficients A_1, A_2, and A_3 are given below for three angles of attack:

Angle of attack, deg	A_1	A_2	A_3
10	0.97	7.3	-4.8
15	.51	6.5	-5.6
20	.71	3.0	-2.0

Comparisons of predictions from equation (12) with the data shown in figure 13 reveal that the mode of the variation with submergence Froude number is very well represented. However, the magnitude of the difference is appreciable because the limit of C_s for $F_h \to \infty$, namely $C_L(\alpha,0)$ is too large. This suggests that this intercept value should be modified for aspect-ratio effect.

It appears from a consideration of the data at extreme Froude numbers for $10 \lesseqgtr \alpha \lesseqgtr 20$ that the difference in the cavitating-section coefficient and the side-force coefficient is insensitive to the angle of attack and that this decrement can be attributed to the effect of geometric aspect ratio. A plot of this difference, namely,

$$\Delta C_s(A) = C_L(\alpha,0) - C_L(\alpha,\infty) \tag{13}$$

where $10^\circ \lesseqgtr \alpha \lesseqgtr 20^\circ$ is given in figure 14. Use of this correction then gives an interpolation formula for the side-force coefficient (over a range of Froude numbers and angles of attack for which full ventilation is obtained) in the form

$$C_s\left(\psi,F_h\right) = \left(C_L(\alpha,0) - \Delta C_s(A)\right)\left(1 + \frac{A_1}{F_h^2} + \frac{4}{3}\frac{A_2}{F_h^4} + \frac{2A_3}{F_h^6}\right) \tag{14}$$

Correlation with the measured values of C_s over the range of these data is shown by the points given in figures 12(a) through 12(c). This tentative result indicates how the side force may be derived from the lift of the fully cavitating section and that the aspect-ratio correction can be made on the lift coefficient at $\sigma = 0$.

Gross Effect of Thickness Distribution on Side Forces

in Fully Ventilated Flow

In a fully ventilated flow, as in a complete cavity flow, the force on the section depends only on the shape of the wetted side, generally the so-called pressure side of the foil. The shape of this side, as determined by comparison with a straight line from the leading edge to the trailing edge (chord line), depends upon the algebraic sum of the thickness and camber ordinates. Thus, the NACA 4412 section used in the experiment had a very flat pressure face and consequently behaved nearly like a cavitating flat plate.

In contrast, the circular-arc foil acted like a cavitating foil having a negative camber ratio $f = t/2 = 0.06$. Because of this the NACA 4412 foil developed much larger side forces than did the circular-arc foil at the same angle of attack. A comparison of the lift coefficients for a flat plate and a negatively cambered circular-arc section can be computed from reference 4. The results are shown in figure 15.

18

This negative force is the result of the suction effect noted on "spoon" bows of stubby-nosed flying boats many years ago. This suction effect can be demonstrated by holding the bottom surface of a teaspoon at a small angle to the stream from a water tap. If allowed to turn about a transverse axis, the spoon will be 'sucked" into the stream. Inasmuch as most struts which pierce the surface are symmetrical, it is to be expected that negative side forces will be developed in full ventilation even though the strut is at a substantial positive angle of attack. Designers can mitigate this effect by keeping the thickness ratio as small as possible.

Another facet of the side force in a ventilated flow is the rate of change of side force with yaw angle about an angle at which a large cavity is found. At $\psi = 20^\circ$, the side-force rate is found to be very insensitive to aspect ratio as shown in figure 16. This fact might be of considerable importance in constructing a theory for fully ventilated flows at low aspect ratios.

In regard to the dynamic stability of a craft using surface-piercing struts or foils, attention is called to the fact that, while the side-force rates with attached flow vary with the geometric aspect ratio in much the same manner as they do for wings with equal aspect ratios, the side-force rates for fully ventilated flows are nearly constant for $0.5 < A < 2.0$. This facet has not been studied theoretically.

The prediction of the lateral force developable on a strut also depends sharply upon the occurrence of ventilation. Therefore, it is necessary to establish criteria or at least a set of bounds within which ventilation may be expected to occur. An attempt to formulate these bounds will be undertaken after a brief presentation of the drag coefficients derived from drag measurements.

Drag-Force Variation

Since the main emphasis of this study was directed toward observation of the flow patterns attending inception and closure of ventilated cavities, little attention was given to the measurement and analysis of drag. Curves of the variation of drag coefficient for the NACA strut at aspect ratios of 1 and 2 are given in figures 17(a) and 17(b), while those for the circular-arc strut are given for $A = 2.0$ in figure 17(c). Inasmuch as the chord Reynolds number range for these was $10^5 \leq R \leq 4 \times 10^5$, the frictional part of the drag may be expected to be affected by the occurrence of laminar flow and laminar separation.

It is interesting to note that upon ventilation the drag drops with the side force since the frictional drag decreases with the aeration of one side and the induced drag follows the reduction of the side force. On the other hand, the form drag arising from the pressure distribution

on the pressure side during ventilation may be larger than the drag obtained with an attached flow. This depends upon the shape of the pressure side. The increase of C_D for the NACA strut at $A = 2$ and $F = 2.0$ may have resulted from a large increase in the form drag which offsets the reduction in frictional and induced drag.

Attention is called to the fact that, although the side force and drag vary with Froude numbers $F > 2$ when ventilation takes place, their ratio is nearly independent of F. This is shown in figure 18 for the NACA strut at $A = 2.0$ for a fixed angle of yaw of 25°. Included for comparison is the curve of C_S/C_D for $\psi = 22^O$ at which there is no ventilation. It is evident that the effect of ventilation is to reduce the side-force-drag ratio by 50 percent. For fully ventilated flow the force coefficients are independent of F for $F > 8$. These limits vary somewhat with aspect ratio.

VENTILATION INCEPTION AND CLOSURE CONDITIONS

Inception of Ventilated Cavities

The upper curves in figures 19(a) through 19(d) show the velocities at which ventilated cavities were observed to form spontaneously behind the NACA strut without end plates at various angles of yaw and aspect ratios of 0.5, 1, 1.5, and 2, respectively. Figure 19(e) shows data for an aspect ratio of 1 with an end plate 8 inches in diameter attached to the lower end.

At an aspect ratio of 0.5, for the speeds and angles tested, only the tip-vortex type of inception was observed. Even at the maximum angle of 28.6^O, the tip-vortex type of ventilation occurred before separation took place. The attainment of this large angle of yaw without separation is attributed to the fact that low aspect ratios permit relief of the negative pressures (which normally exist on the suction side) and thereby reduce the adverse pressure gradients which the boundary layer encounters on the suction side. It was presumed that, if the angle were increased, say to 35°, separation ventilation would preclude ventilation due to the tip vortex.

Comparing figure 19(a) with figure 19(b), it may be seen that at an aspect ratio of 1, separation ventilation occurs before tip-vortex ventilation for all angles above 25.5^O. Below this angle the tip-vortex ventilation develops first. Figures 19(c) and 19(d) show that at angles of 24° and 22° for aspect ratios of 1.5 and 2, respectively, the type of inception mechanism shifts from tip vortex to boundary-layer separation. The increased tendency to favor separation ventilation as the aspect ratio is made larger can be understood on two counts. First, it is known from tests on wings in infinite fluid that the maximum negative

pressure increases in magnitude as the aspect ratio increases. Second, a comparison of figures 19(b) and 19(c) shows that the velocity required to produce tip-vortex ventilation increases as the aspect ratio increases for a given angle. Data for an aspect ratio of 0.5 in figure 19(a) are not directly comparable in this regard because a different type of flow was obtained, namely, that shown in figure 5(b) rather than the usual type as indicated in figure 5(a). In the case of an aspect ratio of 2 (fig. 19(d)) and an aspect ratio of 1 (fig. 19(e)) no tip-vortex ventilation was observed when an end plate was used.

An interesting observation was made in regard to the spontaneous inception of ventilation. In many cases it was possible to achieve the maximum available speed without a cavity when the strut was yawed to an angle 1° less than the minimum yaw found necessary to produce a cavity at high speed. However, upon decelerating from this speed at these fixed yaws, a cavity would form at speeds of the order of one-half of the maximum. •

It also should be emphasized that in any case where the velocity was substantially above that at which a cavity would automatically close, a cavity could be very easily started by a small surface disturbance ahead of the foil, such as the wake of another much smaller body. Such artificially induced ventilation appeared to be of the separation type. The sequence of events following a perturbation of the leading-edge flow suggests that this action separates the surface flow from the boundary-layer flow, allowing air pressure to activate the slow-moving fluid in the separated subsurface boundary layer. (The thin layer of surface flow does not separate in the absence of the perturbation because the longitudinal pressure gradient is zero.) Since the separated subsurface fluid has no predominant horizontal motion with a consequent high inertia, it is possible for the atmospheric pressure to force this fluid downward. As the face of this region moves forward, it is conjectured that the boundary layer continues to separate because this "front" is at a higher pressure than the region into which it is moving.

The implication of these observations is that cavities may be expected to form because of debris, seaweed, choppy water, etc. at velocities well below those at which cavities would form spontaneously in clean, still water. Some reservations in regard to scale effects on this triggering by contamination are given in the section on "Studies and Comments on Scale Effects."

Further observations in regard to the role played by separated boundary-layer flow in inception of ventilation will be given in connection with tests made to determine the state of the boundary layer.

The upper curves in figures 19(f) through 19(i) show the velocities at which cavities form spontaneously behind the circular-arc strut for

aspect ratios of 0.5, 1, 1.5, and 2, respectively. The most striking difference between the curves for the circular-arc strut and those for the NACA 4412 foil is that the tip-vortex type of ventilation was observed only at an aspect ratio of 0.5 for the circular-arc foil but was observed for all aspect ratios except A = 2 for the NACA foil. This difference is attributed to the fact that separation occurs at a lower lift coefficient for the sharp-edged circular-arc foil and hence separation ventilation occurs before the tip vortex has gained sufficient strength to aerate.

Another difference in the curves is that the separation-ventilation curves have a long inclined portion for the circular-arc foil which is much less prominent in the curves for the NACA 4412 foil. This probably is due to the separation which takes place at a more distinctly defined angle for the NACA strut, that is, with less variation of the angle at which separation occurs with Reynolds number. Separation and reattachment of flow under certain conditions is a distinct possibility for the circular-arc foil. This phenomenon is believed also to be responsible for the unusual lift-coefficient curves previously discussed. (Similar behavior in the side-force curves of small-scale struts has been reported by Kiceniuk in ref. 9.) A confirmation of this behavior of the boundary-layer flow has been made through the use of a new technique which will be described after the following section.

Natural Closure of Cavities

In view of the observed greater stability of the cavity flow as compared with that of the attached flow, it was decided to determine the conditions at which a ventilated cavity closes naturally, that is, without the introduction of any disturbance. These conditions would then form a lower bound upon the side-force coefficient and Froude number below which ventilation could not be sustained.

Closure curves were determined by fixing the yaw angle with the cavity open and by observing the speed at which the cavity either closed abruptly or was just sustained to the tip of the strut. Partial cavities were observed to persist for somewhat lower speeds. At large angles the cavity closed gradually, whereas, at small angles the closure was more abrupt and well defined. Curves of closure for the NACA strut are shown in figures 19(a) through 19(e).

At low angles of yaw, from -2° to 5°, the experimental data showed more scatter. The cavities were long and thin, resembling thin flat sheets of air streaming off the suction side of the foil. For such cavities surface tension may play a role in the closure condition. This was due to the spray sheets which tended to coalesce and form a seal over the cavity. In this case the air may be bled from the cavity gradually without replenishment. The spray sheets were observed to oscillate under the variable suction pressure developed by the sealed cavity as its air

C-476

was bled away. Under such conditions the closure was erratic, and scaling of the results was affected by surface tension which maintained intact sprays in small-model tests.

Cavities on the NACA strut at an aspect ratio of 1.5 (fig. 19(c)) could be maintained on the suction side down to yaw angles of -2°. In this case a further reduction of the angle to -3° allowed the formation of a cavity on the pressure side of the foil. Thus, for this foil it appeared that there was a very small range of angles, if any, in which no cavities could be maintained. Furthermore, the maximum velocity required was only 16.4 feet per second which corresponded to a chord Froude number of 5.7.

The velocities for spontaneous closure of cavities for the circular-arc foil are shown by the lower curves in figures 19(f) through 19(i). They are similar to those for the NACA 4412 strut. At high angles of attack the same pattern of increasing minimum velocity required to maintain a cavity with increasing depth is noted. In the case of the circular-arc foil, the flat portion of the curve associated with fully developed separation extended to smaller angles than it did for the NACA 4412 foil. At the same time the minimum angle at which a cavity could be maintained using an available maximum velocity of 30 feet per second was 5°, whereas, it was -2° for the NACA foil.

Since the circular-arc foil is symmetric, no cavities could be maintained by the available velocity of 30 feet per second within a range of angles of yaw from -5° to 5°. This is in contrast with the results for the NACA strut where a cavity could be maintained for all angles except possibly a small range of less than 1° with velocities below 17 feet per second. The reason for this contrasting behavior is thought to be found in the wide differences in the shape of the pressure sides of the two sections. In the case of the 4412 section, which has virtually a flat pressure face, the fluid leaves the trailing edge in a path whose radius of curvature is very large. Hence, its motion maintains a cavity even at small angles of yaw. On the other hand, the fluid particles leaving the trailing edge of the circular-arc section embark on a path whose initial radius of curvature is much smaller, being only about 2 chord. The particles "shed" from the pressure side coalesce with those from the leading edge on the suction side, thus closing the cavity at a short distance from the trailing edge. The short cavity closes easily as compared with the lengthened cavity supported by the flat-faced NACA 4412 section.

Bounds of Side-Force Coefficient and Froude Number for

Existence of Ventilated Cavities

The fact that atmosphere-connected cavities close naturally provides a means for obtaining the upper bounds of the side-force coefficient

and Froude number for which closed or unventilated flows are possible. Beyond these limits ventilation may or may not occur, depending upon a number of things which are not yet well understood. Below these limits ventilation certainly cannot be expected to exist since, if a cavity is imagined to be produced, it will immediately close by itself; that is, it cannot be sustained. Thus, above these limits the attached flow tends to be unstable and below them it is stable with regard to inception of ventilation.

A plot of the side-force coefficients obtained from the unventilated data under the conditions at which the cavities were observed to close is given in figure 20 as a function of the submergence Froude number at closure. It appears that the data fair into an asymptotic line given by

$$C_s F_h{}^2 = 5$$

which indicates that the stable range of C_s shrinks toward zero as the submergence Froude number is made larger. While the data for both foils appear to fall into a consistent pattern, it is noted that the effect of aspect ratio or submergence is not accounted for simply by use of the submergence Froude number. Given a Froude number and an aspect ratio, these curves, if available for the section under consideration, will give the value of the side-force coefficient beyond which ventilation may take place and below which ventilation cannot be sustained. Thus for the models tested, these curves render a sufficient condition for stability of the attached flow state. A definite upper bound for the critical side-force coefficient is that at which stall impends. The lack of certainty with regard to predicting stability of the attached flows (on a full-scale prototype) for the values of C_s between these limits follows from the discovery that local laminar separation existed on the suction side of the models tested. Upon small perturbation of the free surface, air intruded into these regions which immediately led to a change to the completely ventilated pattern and not merely to a replacement of the separated water by air. One may then reasonably ask: Will a prototype strut at much higher Reynolds number with presumably no laminar (or turbulent) separation regions be unstable in this region of C_s below stall and above $5F^{-2}$? A conjectural answer to this is that the attached flow about the full-scale strut would be more stable to small disturbances than the model (with its patch of separation), but it must be basically unstable to large disturbances since the entirely different, completely ventilated flow can exist as another regime in this range of C_s and Froude number as demonstrated by these model tests. In all probability the disturbance may have to be large enough to cause momentary stall-type separation. Since the model behavior was found to be dependent on separation in a C_s region where none was expected, it was decided to study the main characteristics in a preliminary fashion as described in the following section.

STUDIES AND COMMENTS ON SCALE EFFECTS

NACA Technique for Determining Regions of Separation

The sensitivity of a strut to ventilation by perturbation of the surface flow near the stagnation zone at angles of yaw well below those for stall (or extensive boundary-layer separation) may well be limited to models operated at low Reynolds numbers. Recent preliminary studies conducted by the NACA Hydrodynamics Division also showed that ventilation can be triggered by a disturbance near the leading edge of a surface-piercing dihedral hydrofoil. However, the NACA tests have gone further to demonstrate that, for every condition in which ventilation could be induced, the boundary layer prior to the induction was separated. After the surface was disturbed, atmospheric air was observed to displace the low-energy fluid in the separated region and cause a long ventilated cavity to develop. The leading edge of the cavity separation remained near the location of the leading edge of the boundary-layer separation that existed in the unventilated flow.

Attempts to predict the susceptibility of a strut on surface-piercing hydrofoils to ventilation through small-model tests should always entail a determination of the state of the boundary-layer flow through the use of some technique such as the oil—ultraviolet-light method. Identification of the state of the boundary-layer flow over the suction side was made by this method. The oil was applied by hand to the model which was then towed. Areas of separation were revealed when the model was viewed under ultraviolet light under which residual oil fluoresces. The regions of separated flow appeared as white or milky areas. In the case of the NACA experiment, this study revealed that the boundary layer separated in a laminar bubble over the central portion of the chord (the NACA hydrofoil had a mean chord of 1.75 inches) and reattached with transition to turbulent flow at about the 3/4-chord point. It also was observed that a thin strip of completely attached flow existed at the juncture with the free surface so that the separated region appeared as shown in figure 21 when the ventral strut was viewed from above. Disturbances made near the leading edge led to aeration of the aftermost point and the air subsequently filled only the region occupied by the laminar separation.

This phenomenon of local separation and reattachment may be expected to occur frequently in the model-scale range of Reynolds numbers $10^5 < R < 10^6$ and may be expected to be largely absent in the full-scale range. The force coefficient for ventilation in models will be well below that for stall because of this occurrence of a partially separated flow. Thus, inception conditions found from model experiments are expected to be generally pessimistic, that is, to give smaller values of C_S than will be obtained in the prototype. The

observations made by the NACA indicate that turbulence should be stimulated on models of struts or foils being tested for susceptibility to ventilation. As a consequence of these revealing experiments it was decided to conduct similar inspections of the boundary-layer flow on the strut models employed in the Experimental Towing Tank experiments.

Boundary-Layer Tests and Results

Prior to using the oil technique for observing the boundary-layer-flow states it was decided to use turbulence-stimulating devices in order to ascertain whether the angle and speed conditions required for inception by boundary-layer separation could be altered. A sand strip having a width of 1/4 inch and extending from the lower tip to within 0.10 inch of the calm-water intersection (A = 2.0) was applied to the NACA 4412 strut model. The average sand grain diameter was about 0.030 inch.

Tests showed the onset of ventilation occurred at 19° whereas the bare strut ventilated at 22°. As a result it was concluded that the sand strip was too heavy and, instead of its delaying the laminar separation, turbulent separation was being induced by the strip. A fine trip wire 0.010 inch in diameter was tried and produced about the same results. It was still possible to trigger ventilation at a yaw angle of 15°, the major observable difference being that the front of the ventilated cavity was located at the wire, whereas without the wire the cavity leading edge was situated at about the 1/4-chord point.

Determination of the state of the boundary-layer flow next was attempted through the use of the oil—ultraviolet-light technique described above. Sketches of the regions of separated flow with and without the trip wire on the NACA 4412 foil are given in figure 22. Here it can be seen that, in general, the addition of the trip wire provides more separation near the trailing edge which accounts for the small angle at inception. More important is the fact that the model exhibited a laminar separation without the wire so that susceptibility of this strut for larger scales to triggered ventilation may not be nearly so great as indicated by the above-described experiments. This question requires further experimentation either with the same size model employing effective boundary-layer stimulation or with a geometrically similar model of a larger size.

The fact that the ventilation region extended to about the 1/4-chord position without a trip wire appears to check with the position of the leading edge of the separated flow as shown by the sketches on the right side of figure 23. However, if aeration is started through the separated region at the trailing edge, it would seem necessary for the cavity to spread over the region of nonseparated flow between the trailing edge and the region in the vicinity of the midchord. Therefore, it is not

yet clear whether the final boundaries of the ventilated flow will be located at the boundaries of the separated flow.

A brief investigation of the flow on the circular-arc strut was made to ascertain if the odd behavior in the side-force curves could be correlated with an alteration in the boundary-layer flow as the chord Reynolds number is varied. The oil method was applied and the strut towed at a yaw of 10° at Reynolds numbers of 0.95×10^5 (F = 2) and 2.9×10^5 (F = 6). The sketches made of the regions of separation as given in figure 23 show a large change in the boundary-layer conditions when the Reynolds number was increased at a constant yaw of 10°. Clearing the large separated zone near the trailing edge accounted for a decrease in side-force coefficient at the higher Reynolds number. Presumably, the separation at the low Reynolds numbers provided an effective camber and, therefore, a larger side force.

It should be expected that the final forward boundaries of the ventilated region will roughly coincide with those of the region of boundary-layer separation without ventilation because the pressure in the separated zone is nearly constant. Hence, the flow velocity on the boundary of the separated zone is constant in magnitude. Thus, the existence of a surface of constant velocity (at least at a fixed depth) already is established and the position of this surface may not vary if the separated flow is replaced by air at atmospheric pressure. This concept of "static" replacement of the boundary-layer fluid may be expected to work at fairly low speeds, but at high speeds it is conjectured that the onset of ventilation may be so violent as to introduce dynamic effects. These bring about a considerably different position of the ventilated cavity. This point may merit further study.

At the larger angle of yaw ($\psi = 15^\circ$) at which the side-force coefficient (in the unventilated state) showed no variation with speed, the boundary layer exhibited only a small change in the separated area as is indicated in the lower part of figure 23. Thus, the behavior of the force coefficient and boundary layer were consistent. The fact that the sharp-nosed circular-arc section did exhibit separation at the leading edge with subsequent reattachment should be expected particularly at these low Reynolds numbers. Again, the front of the ventilation for this case also coincided with the front of the separated zone, namely, the leading edge.

Surface Tension as Another Factor in Scaling Ventilation

It may be expected that surface tension which remains virtually the same from model to prototype will prevent the ventilation phenomena from scaling. Work at the University of Minnesota (which is believed to

be unpublished) has shown that the inception and extent of ventilation is dependent upon the Weber number (ratio of surface-tension force to inertia force) for circular cylinders less than 2 inches in diameter over a practical range of Froude and Reynolds numbers. Surface tension may be important wherever the radii of curvature of the surface flow are very small. For example, the local "dimpling" of the surface (Rankine vortices) in the neighborhood of the separated flow at the trailing edge of a strut may be expected to vary with the scale of the flow since the instantaneous radius of curvature of a small dimple will be attended by a relatively large surface-tension force tending to oppose the propagation of this deformation. Surface tension also may be vital in the case of spray sheets which remain solid in model scale, but may break into fine droplets in full scale. In the Experimental Towing Tank tests it is believed that the conditions of closure at small angles of attack may be subject to the influence of surface tension in that both the pressure-side and suction-side sprays remain intact and close over the cavity. This blocks air from entering and the remaining air in the cavity is entrained away. It may well be expected that in full scale these sheets would be broken up into droplets. This effect requires experimentation with larger models and with variation of the surface tension so that the Weber number can be significantly changed.

CONCLUSIONS

As a result of the study of ventilated flows about yawed surface-piercing struts it appears possible to draw some fairly general conclusions. The most important of these are the following:

1. For a given strut and aspect ratio a curve can be drawn of side-force coefficient versus submergence Froude number. This curve defines critical values of both these numbers below which no aerated cavity can be maintained.

2. Above the critical side-force coefficient (at a given submergence Froude number) once a cavity is generated it is maintained.

3. Inception of ventilation at side-force coefficients in excess of the critical values is dependent upon the presence of a separated flow which becomes connected to the atmosphere. The connection to the atmosphere can occur in a variety of ways.

4. The most practical method of incepting a cavity above the critical side-force coefficient on small models is through a disturbance causing a momentary separation of the flow at the juncture of the foil and the free surface.

5. A definite upper bound for the critical side-force coefficient is that at which stall impends.

6. The force coefficient at which ventilation can be initiated will depend, in general, upon the Reynolds number and, in the case of models, will be well below that for stall because of the occurrence of a partially separated flow. Thus, inception conditions found from model experiments are expected to be generally pessimistic, that is, to give smaller values of side-force coefficient C_S than will be obtained in the prototype.

7. At angles of yaw less than those for boundary-layer separation, spontaneous ventilation may be induced by an aerated tip vortex. However, this vortex probably will not exist if the strut is connected to a hydrofoil. This mechanism could be important in the case of ventral foils.

8. Further experimentation employing geometrically similar models at larger Reynolds numbers and effective means for stimulating turbulent boundary layers should be undertaken. A variation of surface tension should be included in this study to determine the effect of this parameter on a cavity closure at low angles.

9. The variation with Froude number of the side-force coefficient (with complete ventilation) can be predicted through the use of a cavitating-foil lift as a function of an effective cavitation index which is simply related to the Froude number.

10. For maximum force effectiveness in a ventilated condition, a symmetrical strut should be as thin as possible.

11. Attempts to predict the susceptibility of a strut on surface-piercing hydrofoils to ventilation through small-scale model tests should always entail a determination of the state of the boundary-layer flow through the use of some technique such as the oil—ultraviolet-light method.

12. In order to postpone the inception of ventilation of surface-piercing bodies which develop lift or side force, it appears advisable to reduce the local side loading near the juncture with the free surface so that the generation of regions of boundary-layer separation will be avoided. This can be done by increasing the chord and, in the case of dihedral foils, by reducing the angle of attack through twist.

13. It is of some importance to note that for unventilated flow the side-force and drag coefficients are independent of Froude numbers greater than 2.0. For fully ventilated flow the force coefficients are independent of a Froude number greater than 8. These limits vary somewhat with aspect ratio.

14. In regard to the dynamic stability of crafts using surface-piercing struts or foils, attention is called to the fact that, while the side-force rates with attached flow vary with the geometric aspect ratio A in much the same manner as they do for wings of equal aspect ratios, the side-force rates for fully ventilated flows are nearly constant for $0.5 < A < 2.0$. This facet has not been studied theoretically.

Experimental Towing Tank,
    Stevens Institute of Technology,
        Hoboken, N. J., November 4, 1957.

REFERENCES

1. Wadlin, Kenneth L., Ramsen, John A., and Vaughan, Victor L., Jr.:
   The Hydrodynamic Characteristics of Modified Rectangular Flat Plates
   Having Aspect Ratios of 1.00 and 0.25 and Operating Near a Free
   Water Surface. NACA TN 3079, 1954.

2. Gongwer, C. A.: A Study of Vanes Singing in Water. Rep. RJM-76,
   Aerojet Eng. Corp., May 3, 1951.

3. Kaplan, P.: Test of Surface Piercing Struts. LR-488, Exp. Towing
   Tank, Stevens Inst. of Tech., Apr. 1953.

4. Hay, Arthur Donald: Flow About Semi-Submerged Cylinders of Finite
   Length. J05, Contract NObs-34006, The David W. Taylor Model Basin
   and Princeton Univ., Oct. 1, 1947.

5. Coffee, Claude, W., and McKann, Robert E.: Hydrodynamic Drag of 12-
   and 21-Percent Thick Surface-Piercing Struts. NACA TN 3092, 1953.

6. Breslin, J. P.: The Hydrodynamic Characteristics of Several Surface
   Piercing Struts. Rep. No. 596, Contract NObs-47790, T.O. 16, The
   David W. Taylor Model Basin and Exp. Towing Tank, Stevens Inst. of
   Tech., Jan. 1956.

7. Wu, Yao-tsu: A Free Streamline Theory for Two-Dimensional Fully
   Cavitated Hydrofoils. Rep. No. 21-17, Contract N6-onr-24420,
   Office of Naval Res. and Calif. Inst. of Tech., July 1955.

8. Perry, B.: Experiments on Struts Piercing the Water Surface. Rep.
   No. E-55.1, Contract N-123s-91875, Naval Ord. Test Station and
   Calif. Inst. of Tech., Dec. 1954.

9. Kiceniuk, Taras: A Preliminary Study of Vertical Hydrofoils of Low
   Aspect Ratio Piercing a Water Surface. Rep. No. E-55.2, Con-
   tract N-123s-91875, Naval Ord. Test Station and Calif. Inst. of
   Tech., Dec. 1954.

(a) Attached flow at $F = 3.63$. Note absence of spray on suction side of strut and surface spray in wake caused by the confluence of flows from pressure and suction sides.
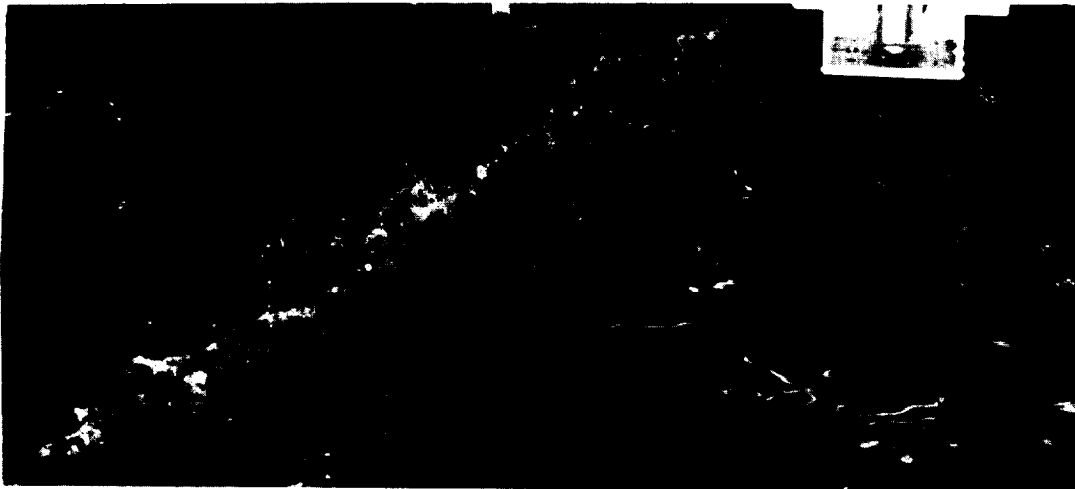
L-58-4271

(b) Ventilated flow at $F = 3.74$. Note presence of suction-side spray and absence of surface spray.

Figure 1.- NACA 4412 foil towed on rotating arm; $A = 1.0$; $\psi = 20^\circ$.
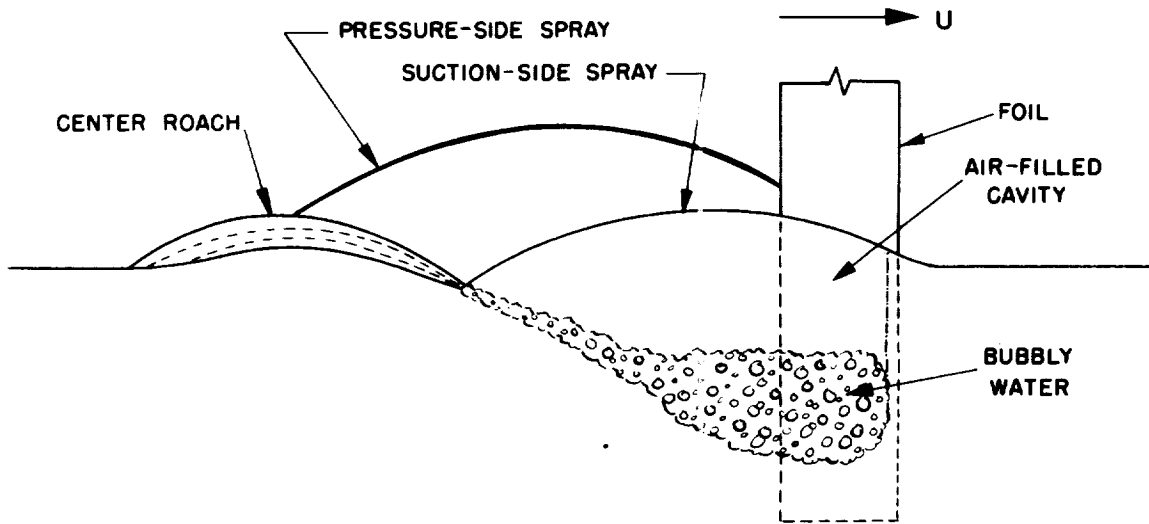
Figure 2.- Partial cavity formed at low Froude numbers and large angles of attack.
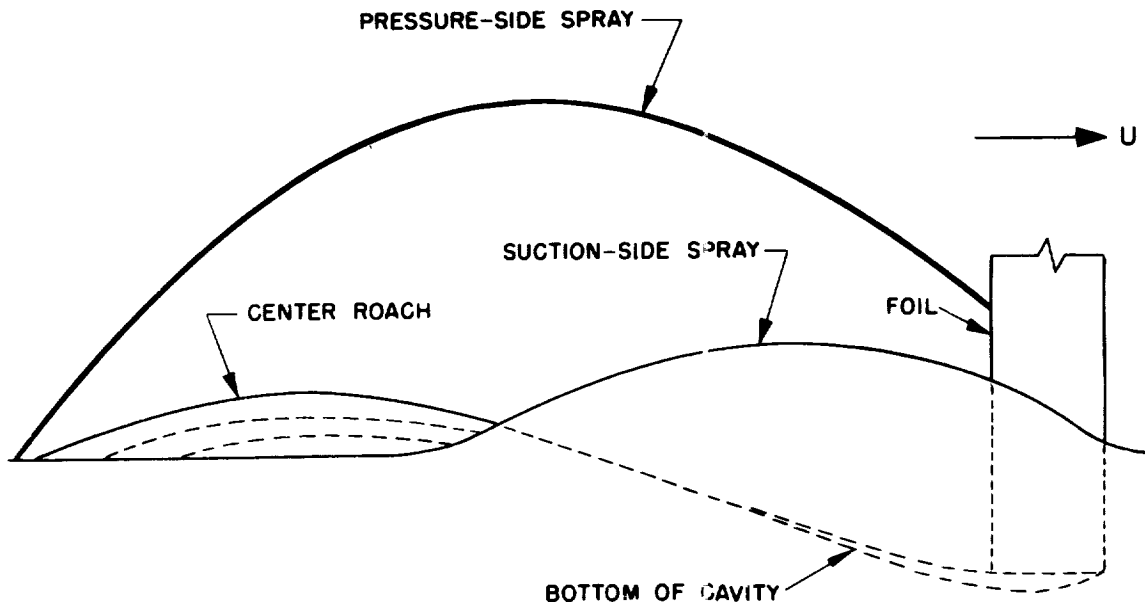
Figure 3.- Typical complete atmosphere-connected cavity.
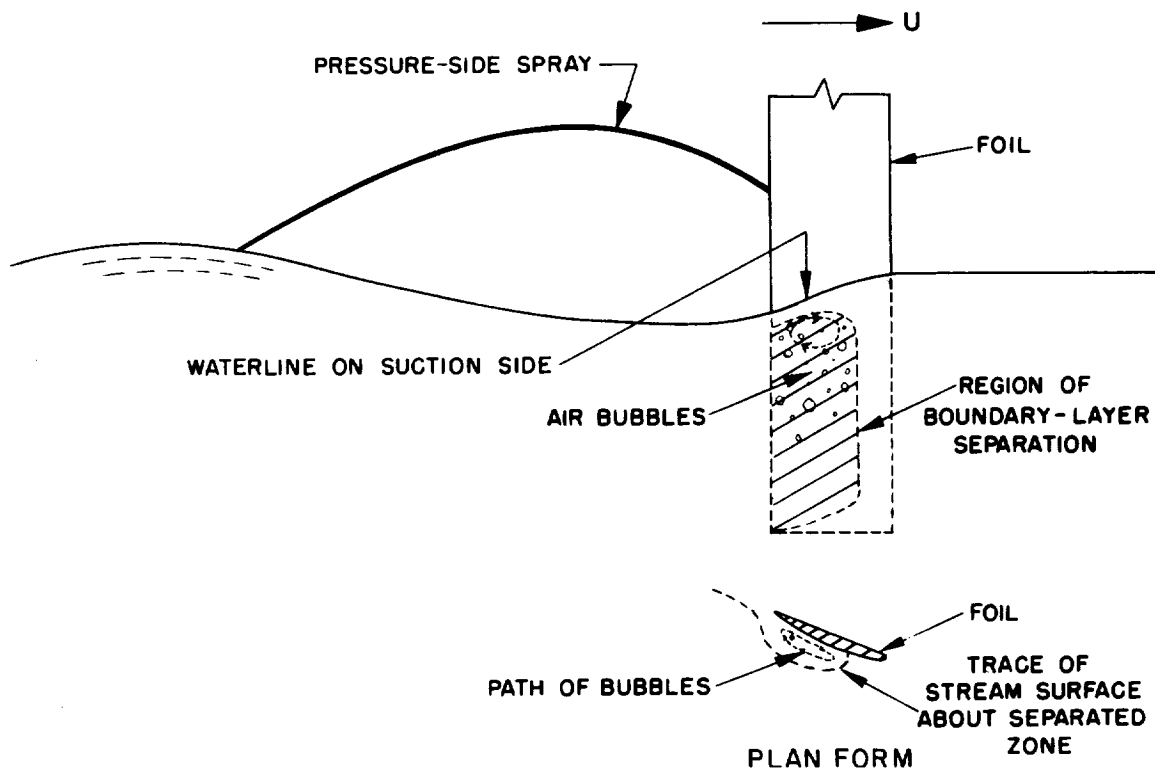
Figure 4.- Conditions at inception of cavity due to separation.
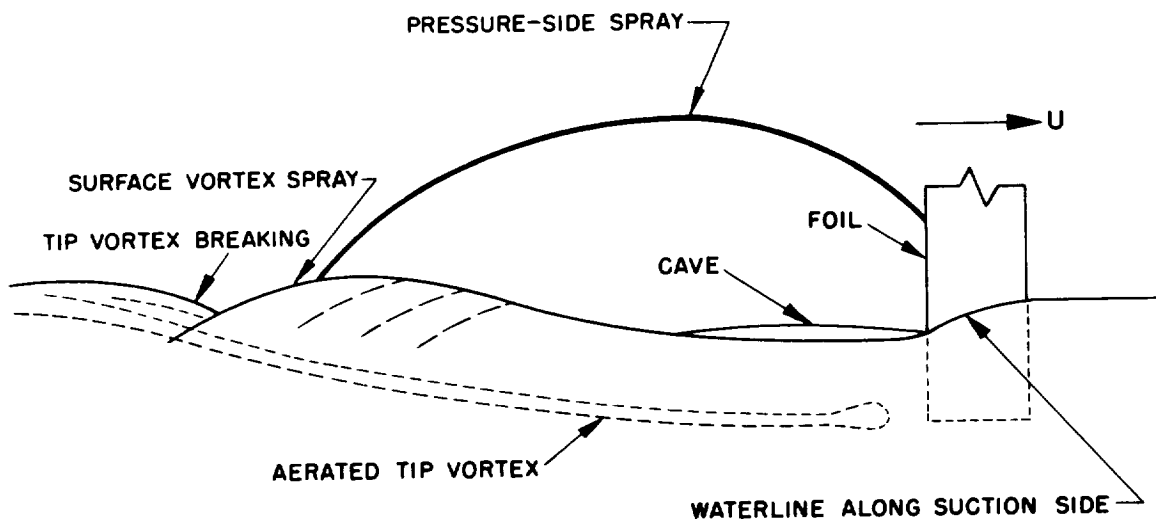
(a) Most typical flow pattern.

Figure 5.- Aerated tip vortex just prior to inception of cavity.
(Cf. fig. 4.)
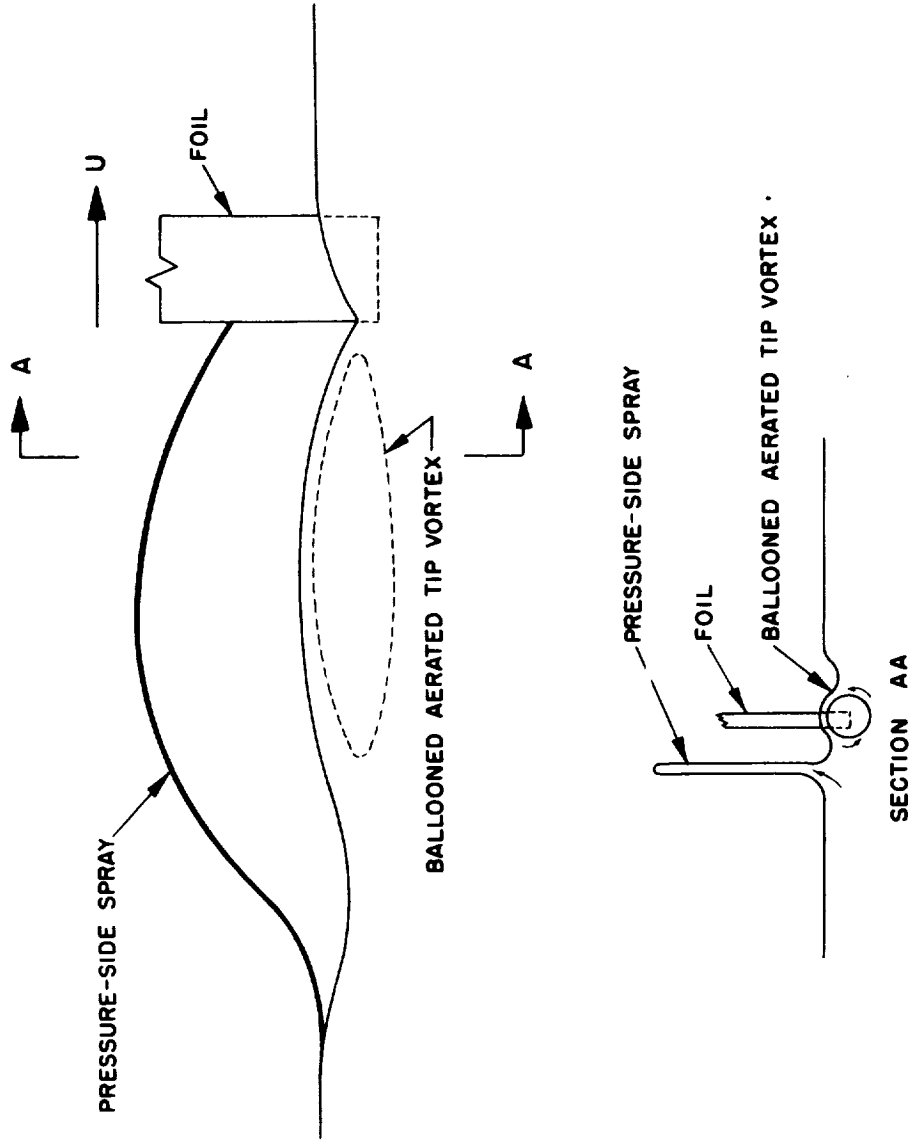
(b) Another flow pattern taken at A = 0.5.

Figure 5.- Concluded.
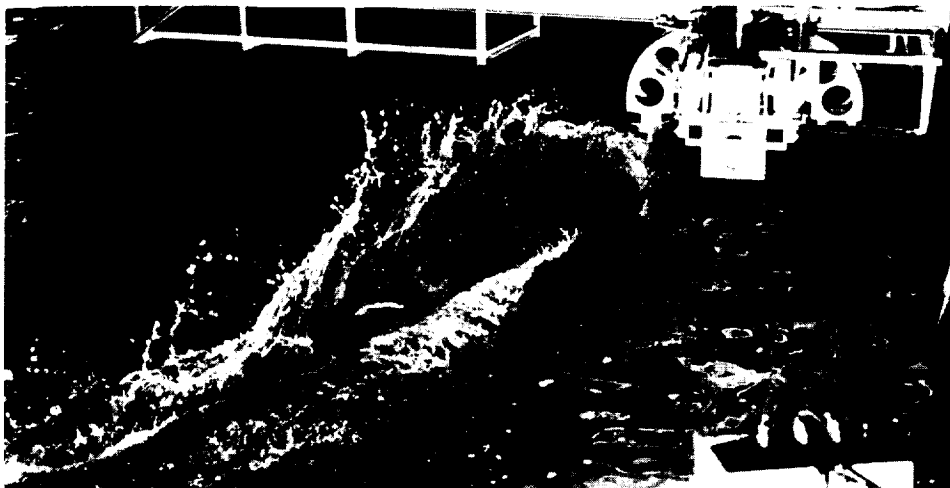
(a) Wake on surface at $F = 6.77$, unventilated.

(b) Underwater view of suction side at $F = 6.77$ showing unattached, aerated lower tip vortex.
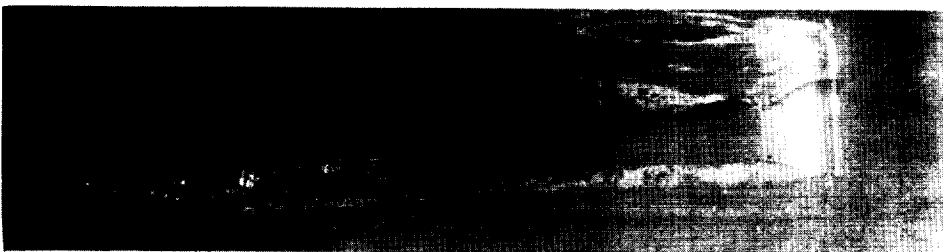
L-58-4272

(c) View at slightly higher speed, $F = 7.38$, showing attached, aerated lower tip vortex prior to producing ventilation of entire suction side.

Figure 6.- Views of NACA 4412 foil with attached flow at high speed, yawed to 20°.
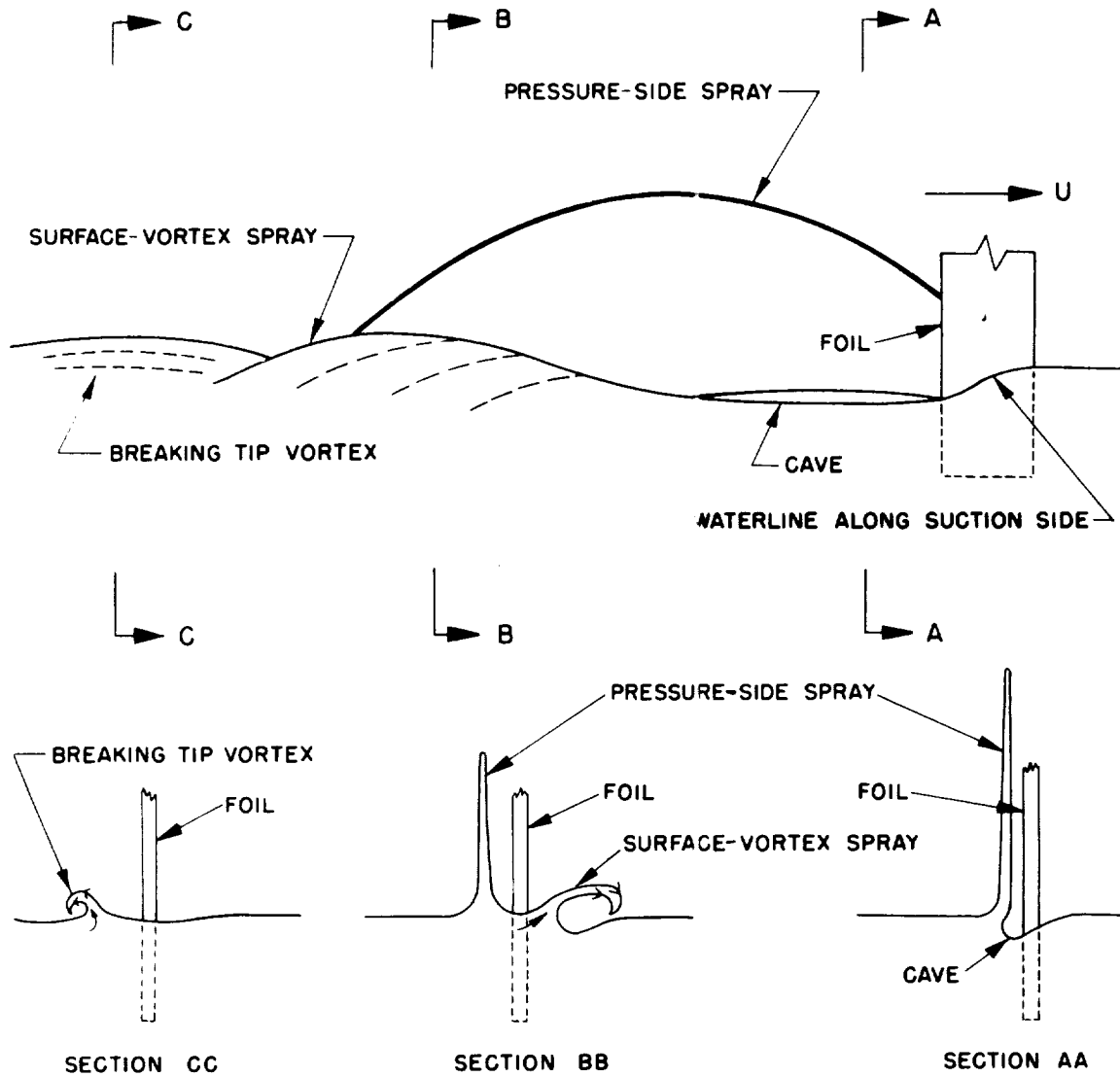
Figure 7.- Typical condition with no cavity at high Froude numbers.
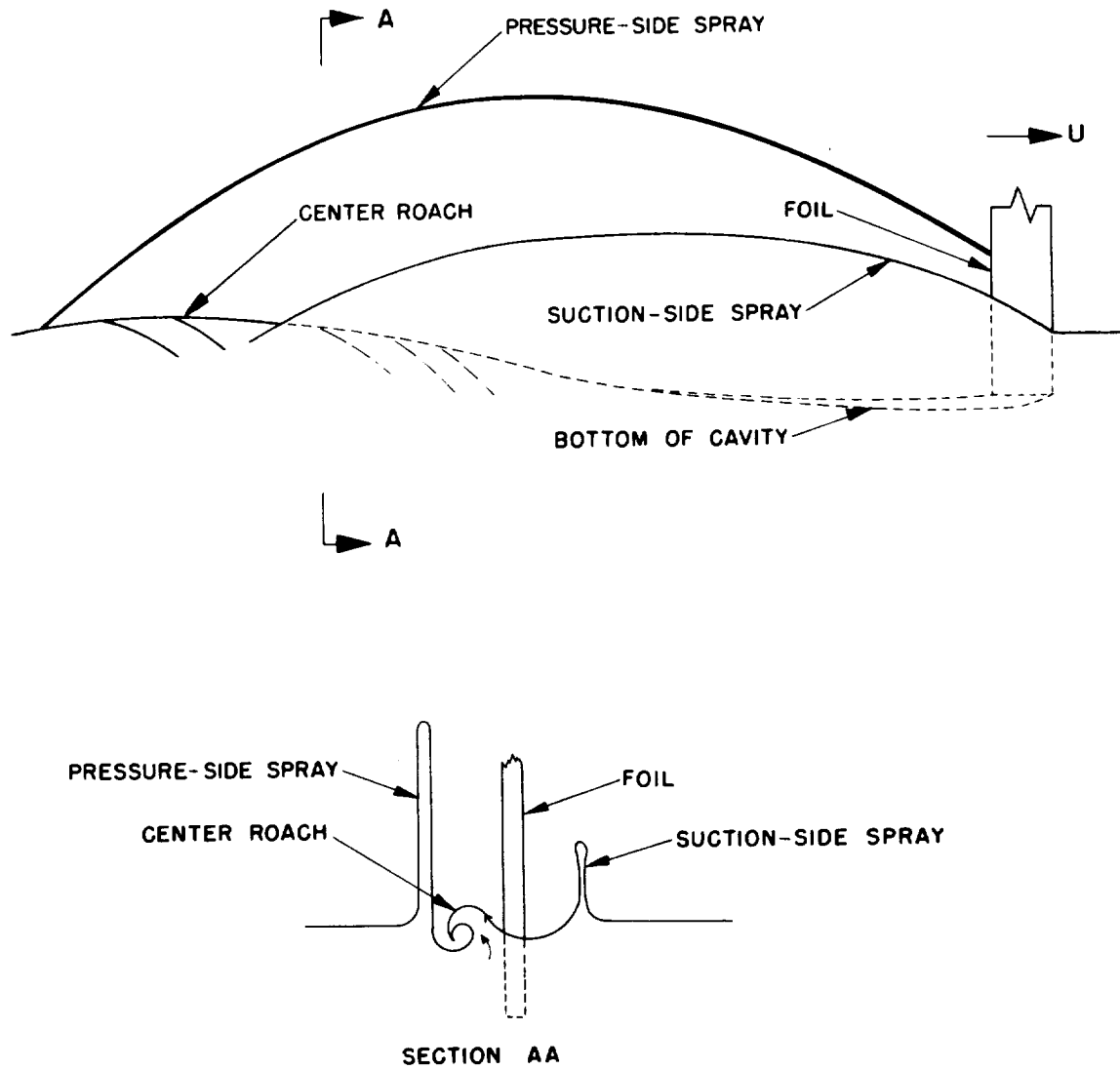
Figure 8.- Form of cavity at high Froude numbers.
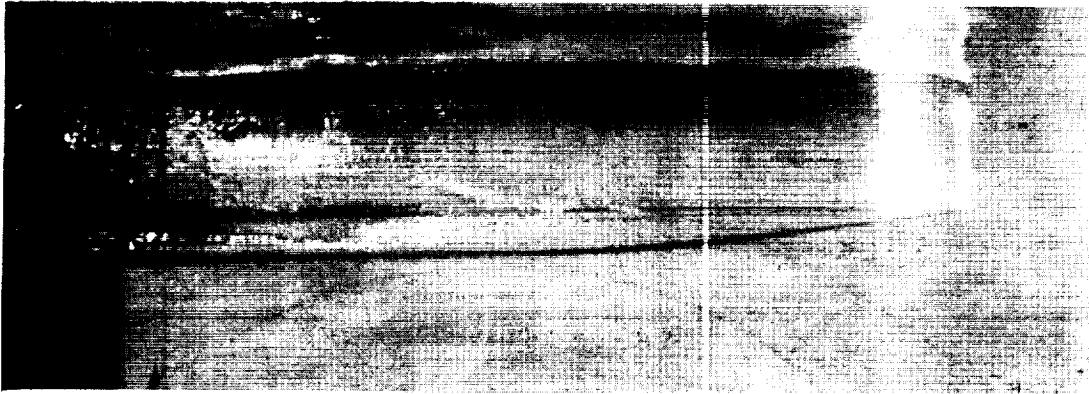
(a) Underwater view at $F = 7.9$.
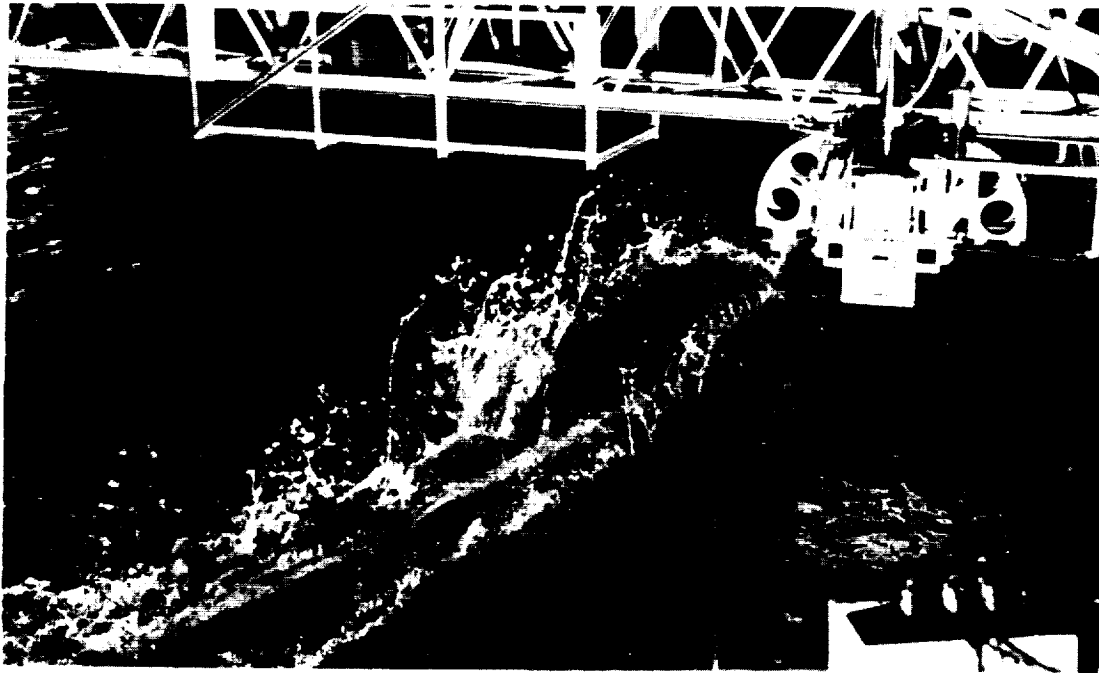
L-58-4273

(b) Rear view at $F = 6.45$.

Figure 9.- Suction side of NACA 4412 foil with full ventilation;
$A = 1.0$, $\psi = 20°$.
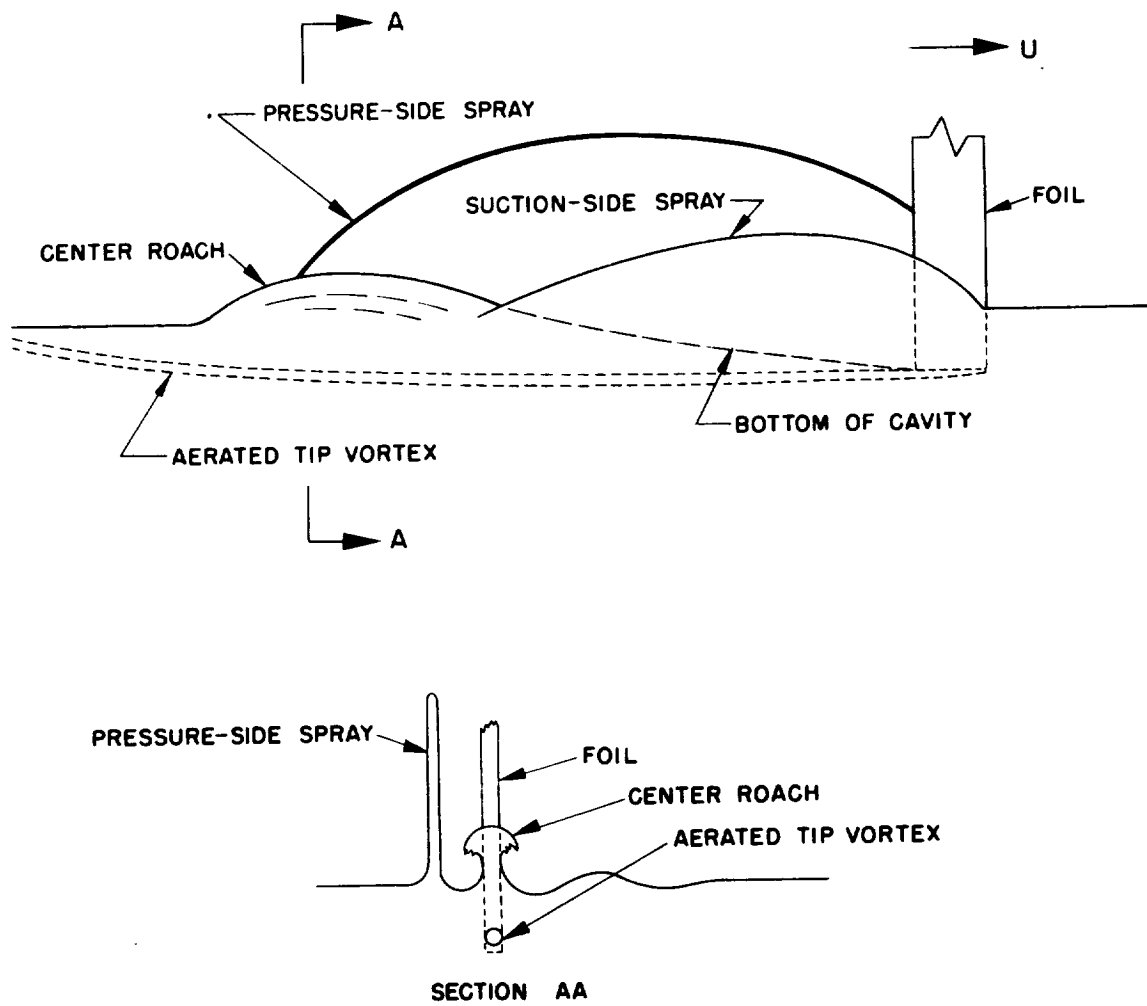
Figure 10.- Form of cavity at medium Froude numbers.

SECTION AA
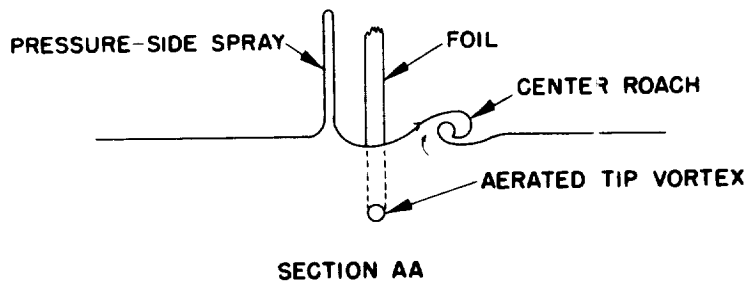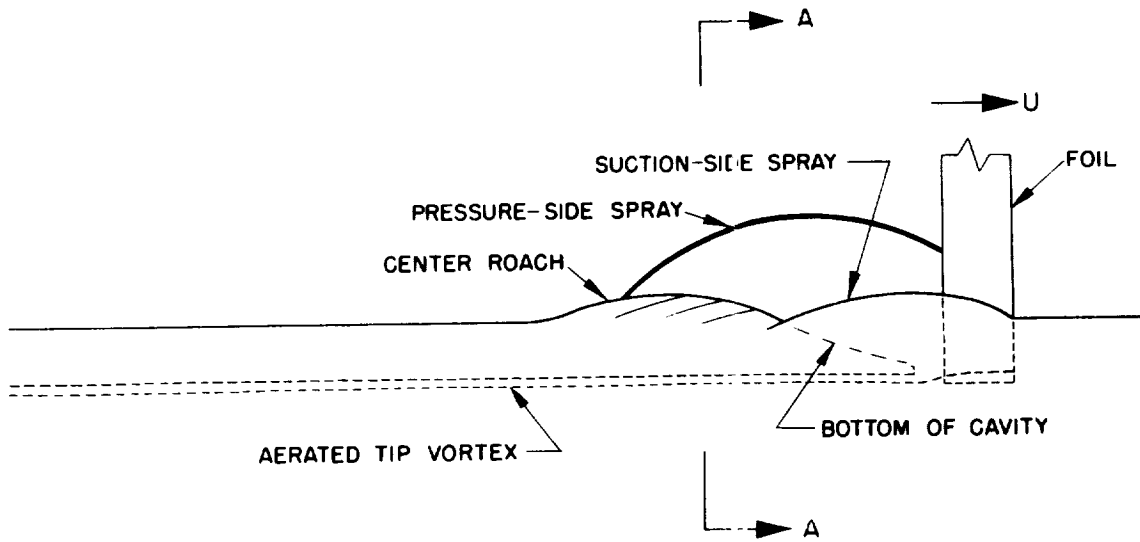
Figure 11.- Form of cavity at low Froude numbers.
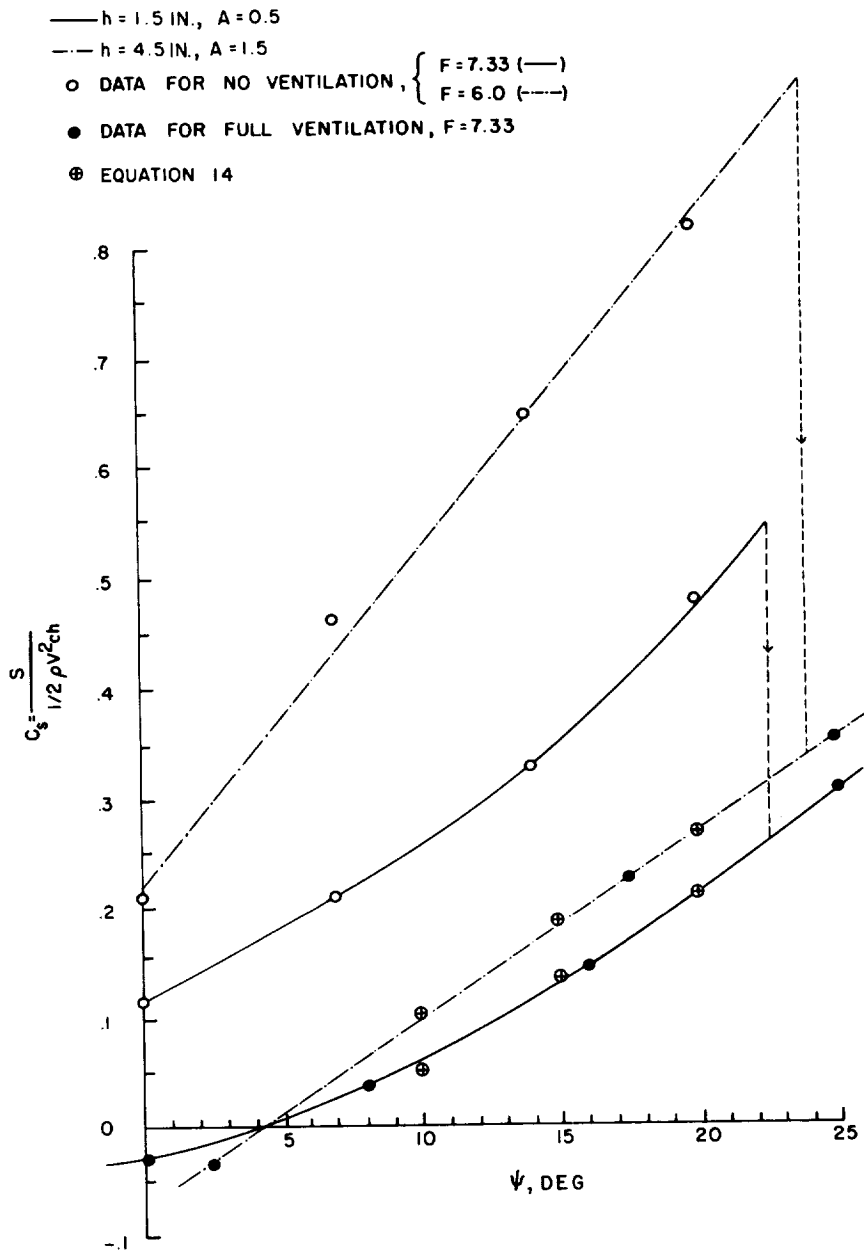
(a) NACA 4412 strut; c = 3.0 inches; h = 1.5 and 4.5 inches;
A = 0.5 and 1.5.

Figure 12.- Side-force coefficients for NACA 4412 and circular-arc
struts. Vertical broken lines on right show angles at which cavi-
ties open spontaneously; those on left show angles at which cavities
close.
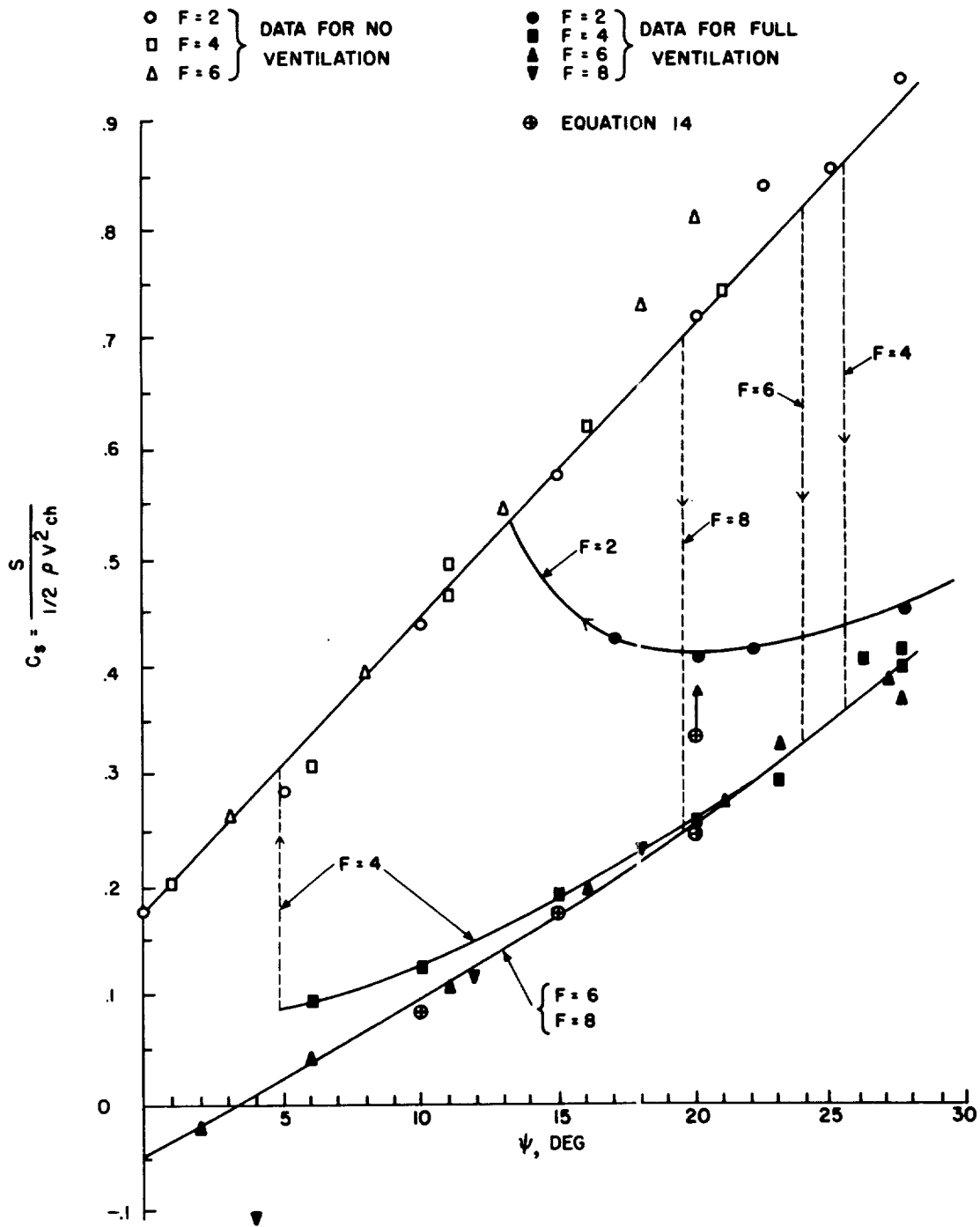
(b) NACA 4412 strut; c = 3.0 inches; h = 3.0 inches; A = 1.0.

Figure 12.- Continued.
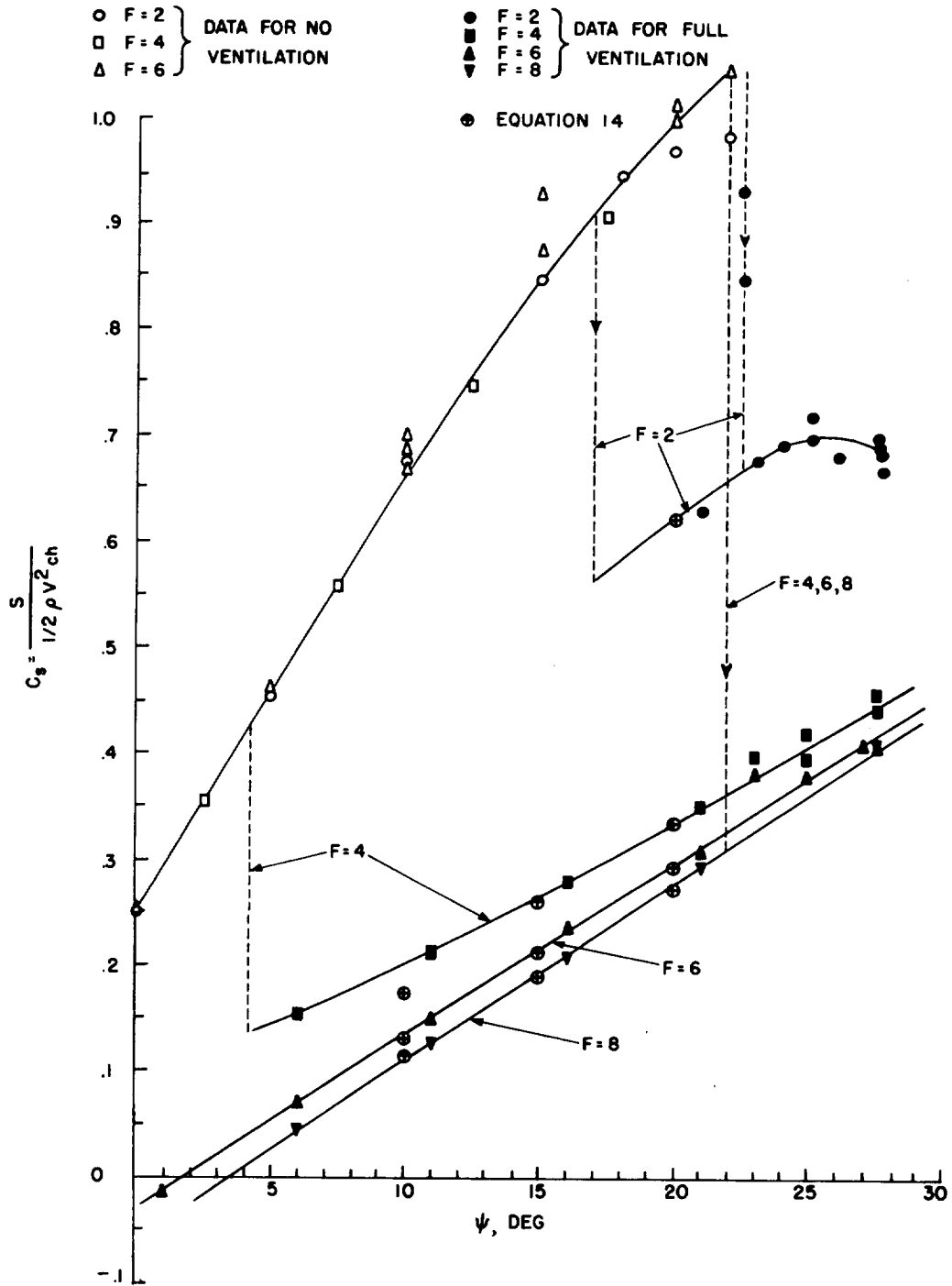
(c) NACA 4412 strut; c = 3.0 inches; h = 6.0 inches; A = 2.

Figure 12.- Continued.

○ DATA FOR NO VENTILATION, F = 8 }
● DATA FOR FULL VENTILATION, F = 8 } BOTH GRAPHS
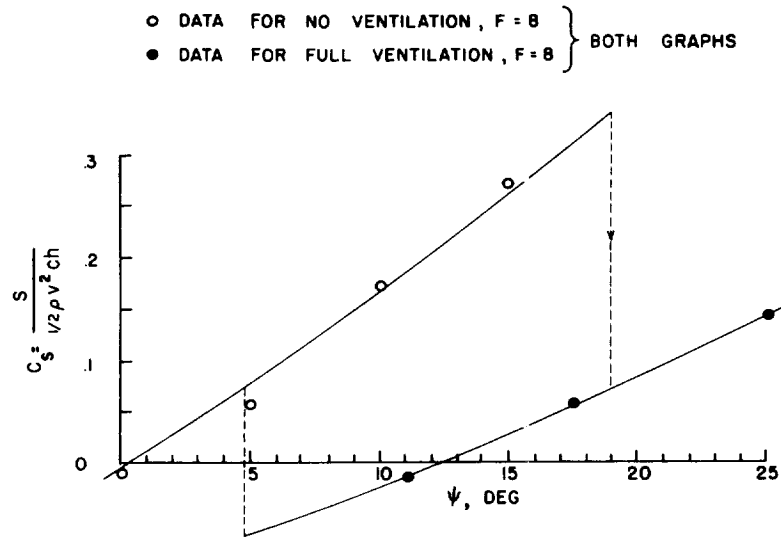
(d) Circular-arc strut; c = 2.5 inches; h = 2.5 inches; A = 1.0.
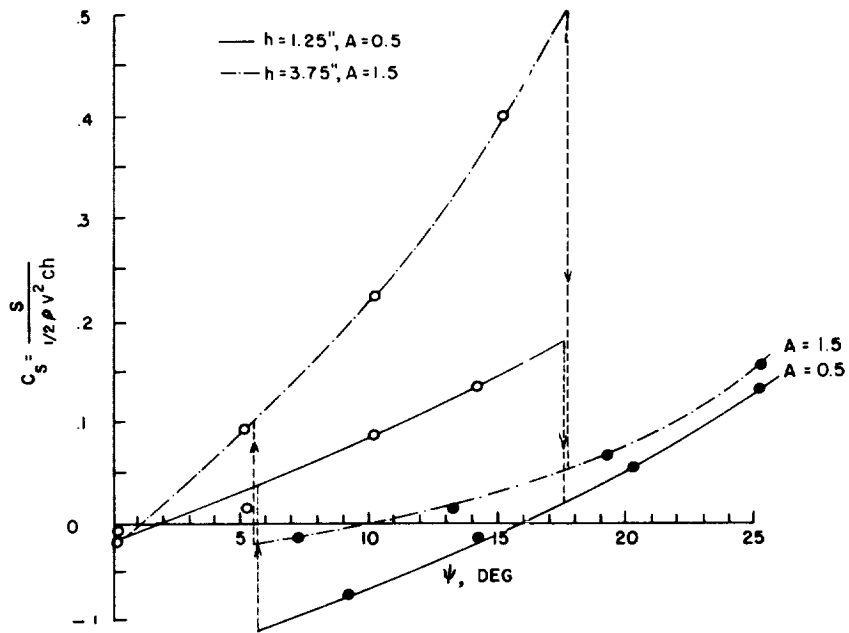
(e) Circular-arc strut; c = 2.5 inches; h = 1.25 and 3.75 inches;
A = 0.5 and 1.5.

Figure 12.- Continued.
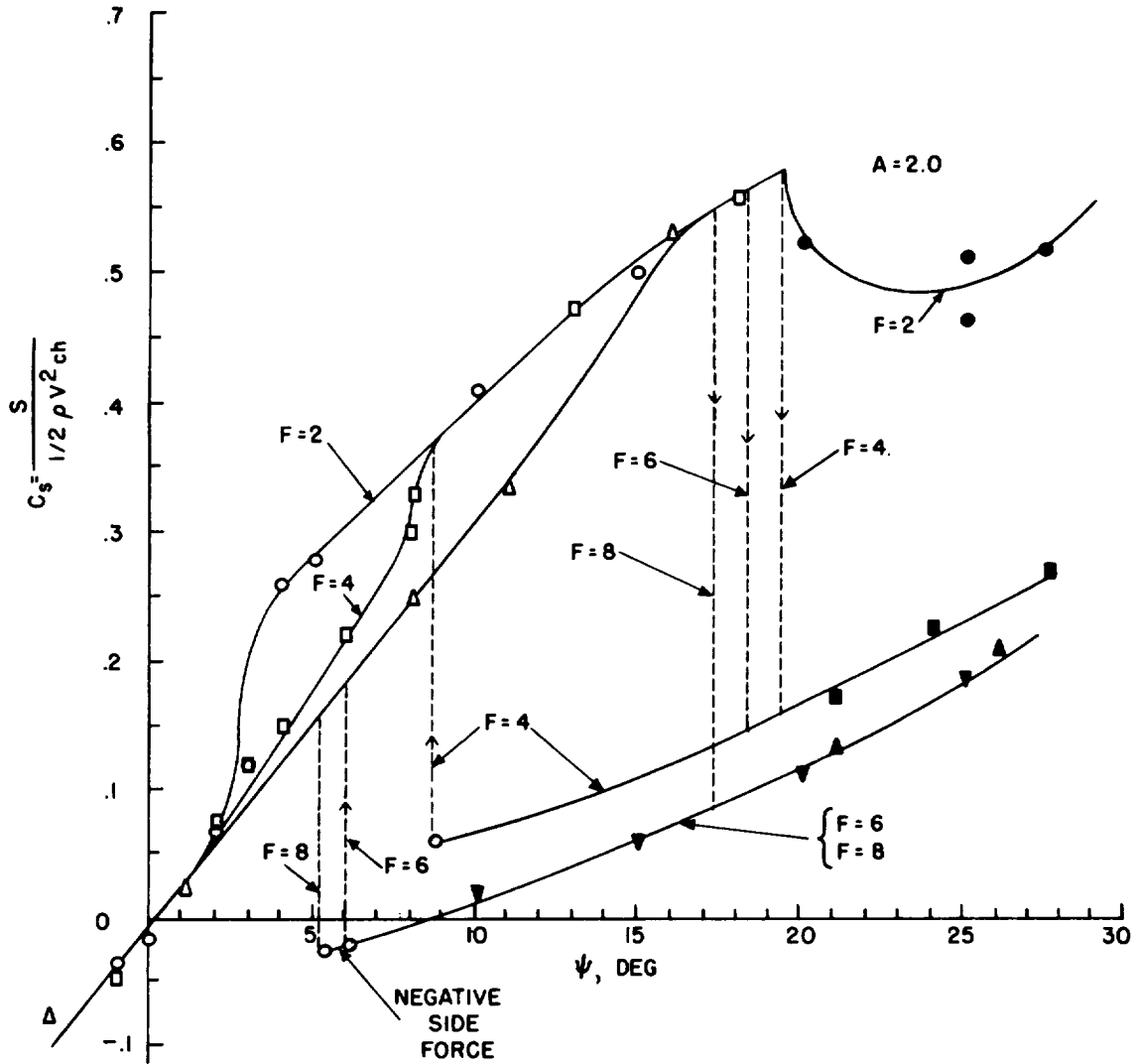
(f) Circular-arc strut; c = 2.5 inches; h = 5.0 inches; A = 2.0.

Figure 12.- Concluded.
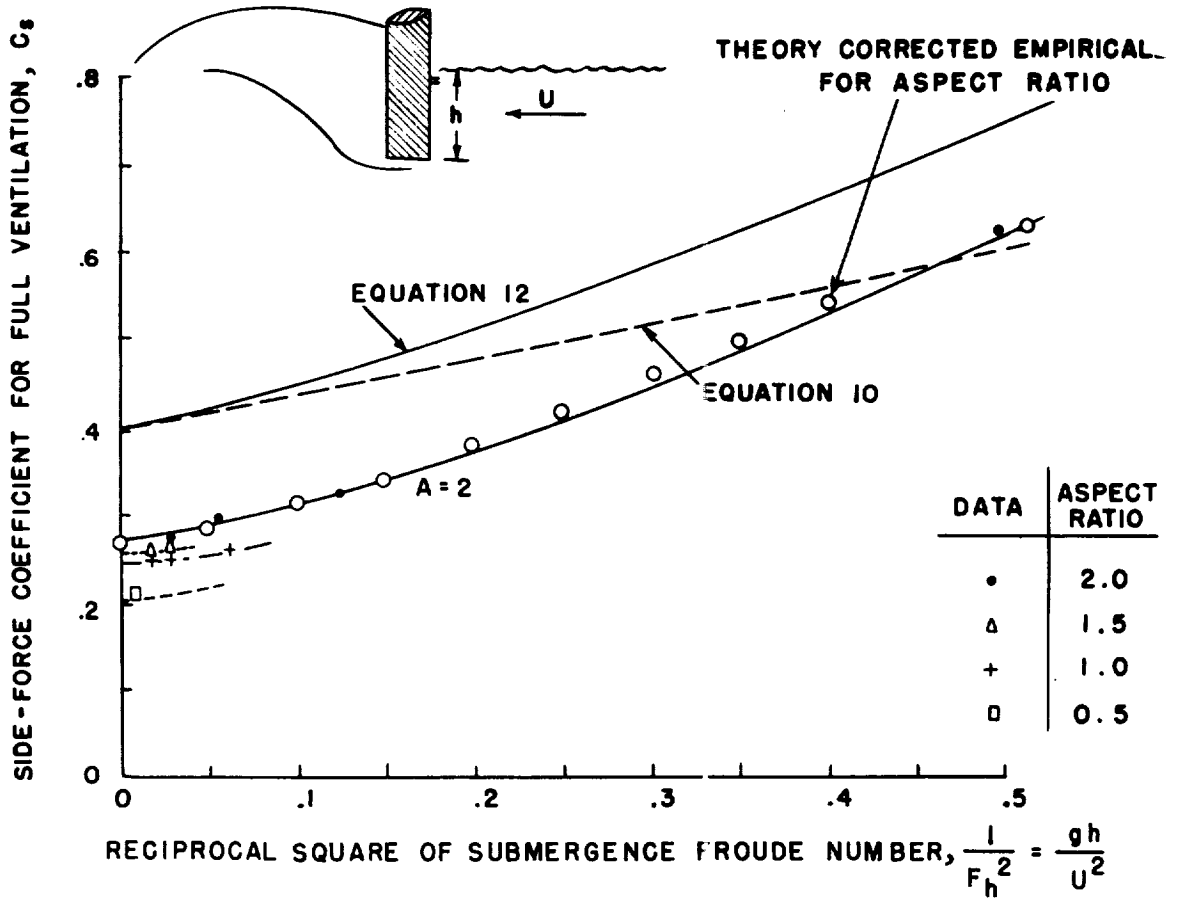
Figure 13.- Variation of side-force coefficient with Froude number and aspect ratio from measurements at $\psi = 20°$.
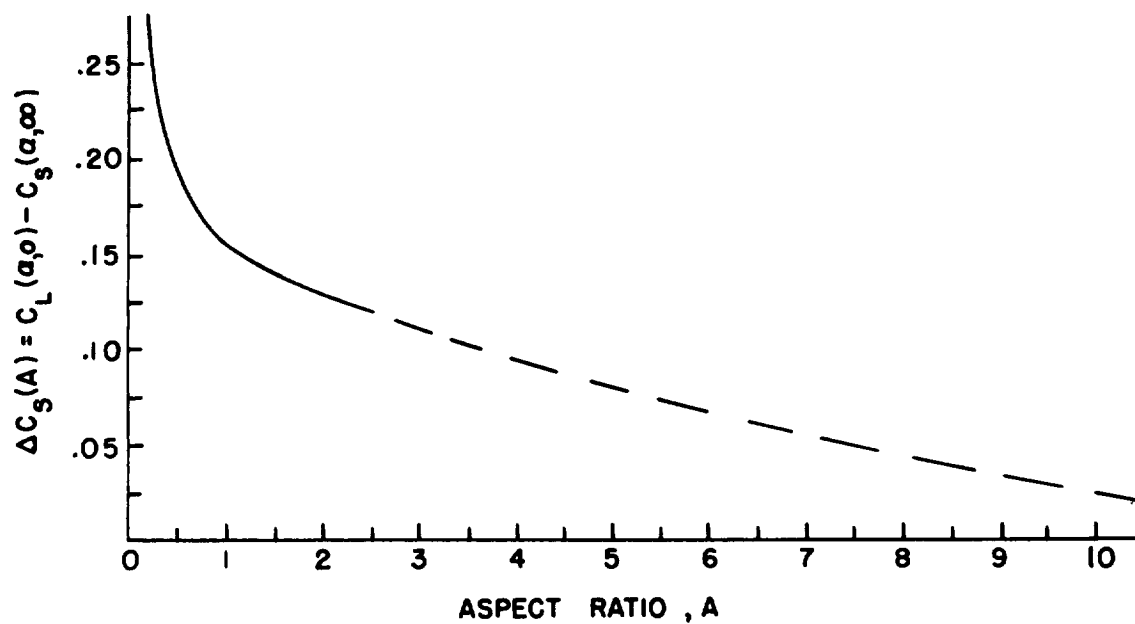
Figure 14.- Correction of side-force coefficient for infinite Froude number for effect of aspect ratio as determined from data.

$$C_s(\psi, \infty) = \left[C_L(\alpha, 0) - \Delta C_L(A)\right].$$
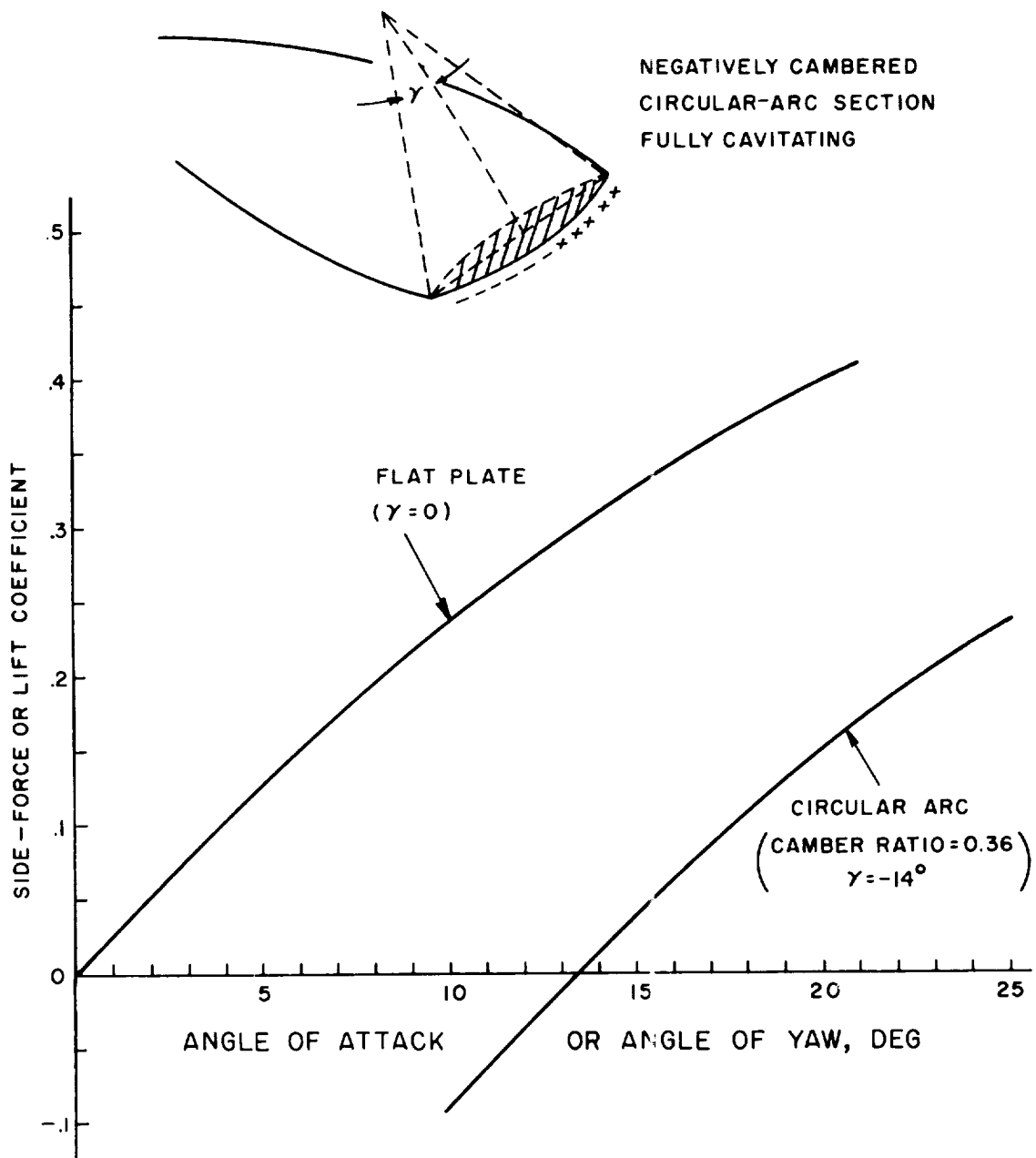
Figure 15.- Theoretical lift coefficients for flat and negatively cam-
bered sections at zero cavitation number computed from formulas in
reference 4.
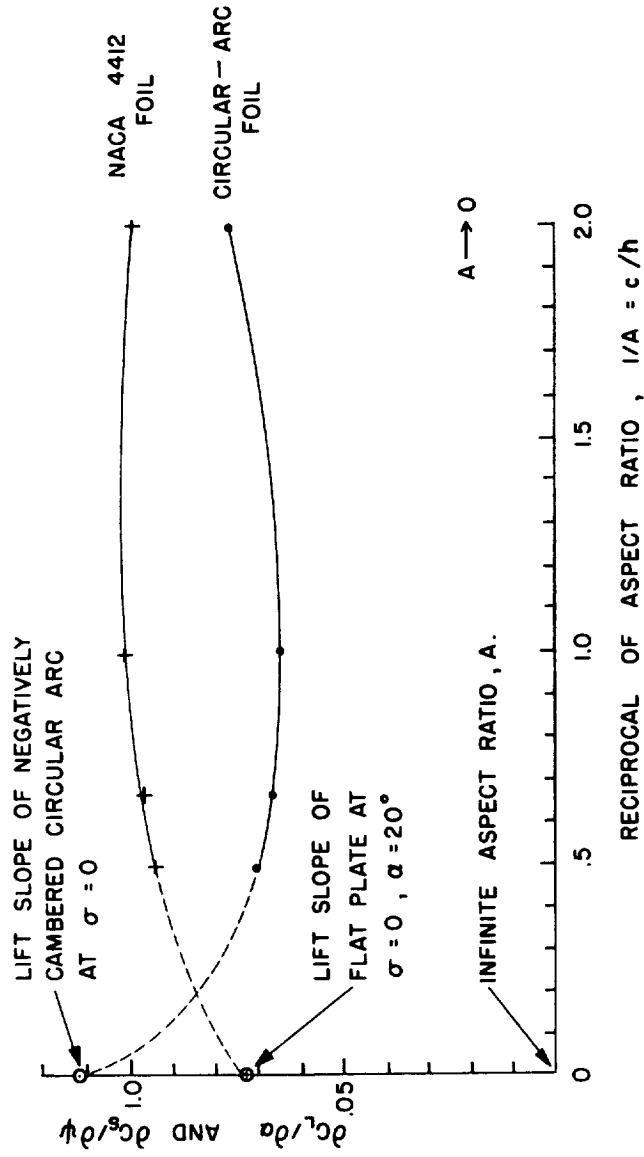
Figure 16.- Variation of side-force-coefficient rate $\partial C_S / \partial \psi$ with aspect ratio as determined from test data at Froude numbers $F \geqq 6$. All rates evaluated at $\psi = \alpha = 20°$.
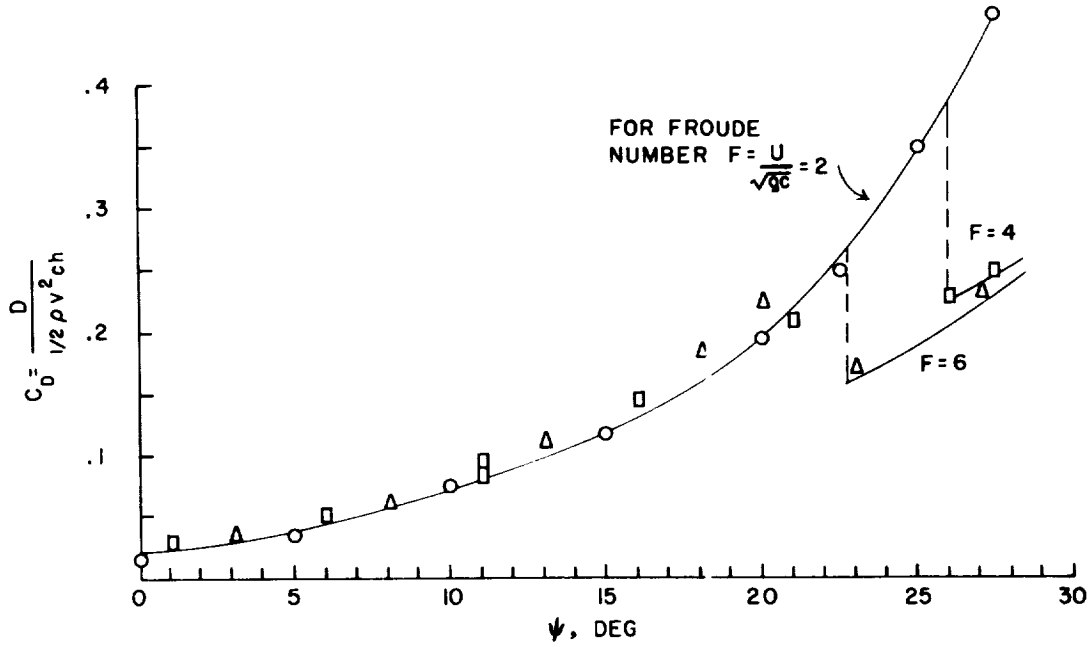
(a) NACA 4412 strut; c = 3.0 inches; h = 3.0 inches; A = 1.
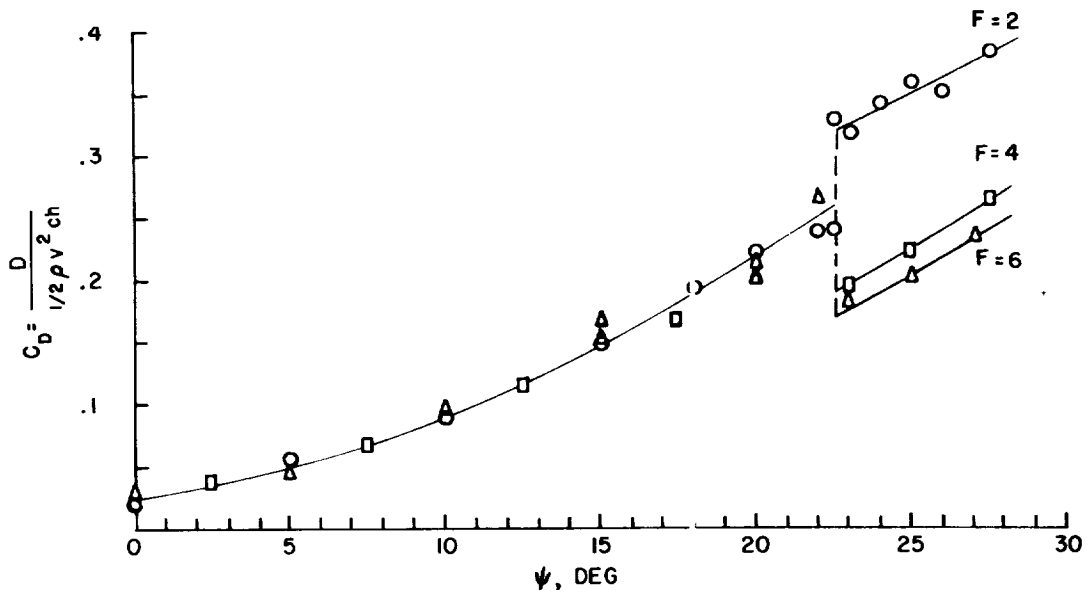
(b) NACA 4412 strut; c = 3.0 inches; h = 6.0 inches; A = 2.

Figure 17.- Drag coefficients for surface-piercing strut..
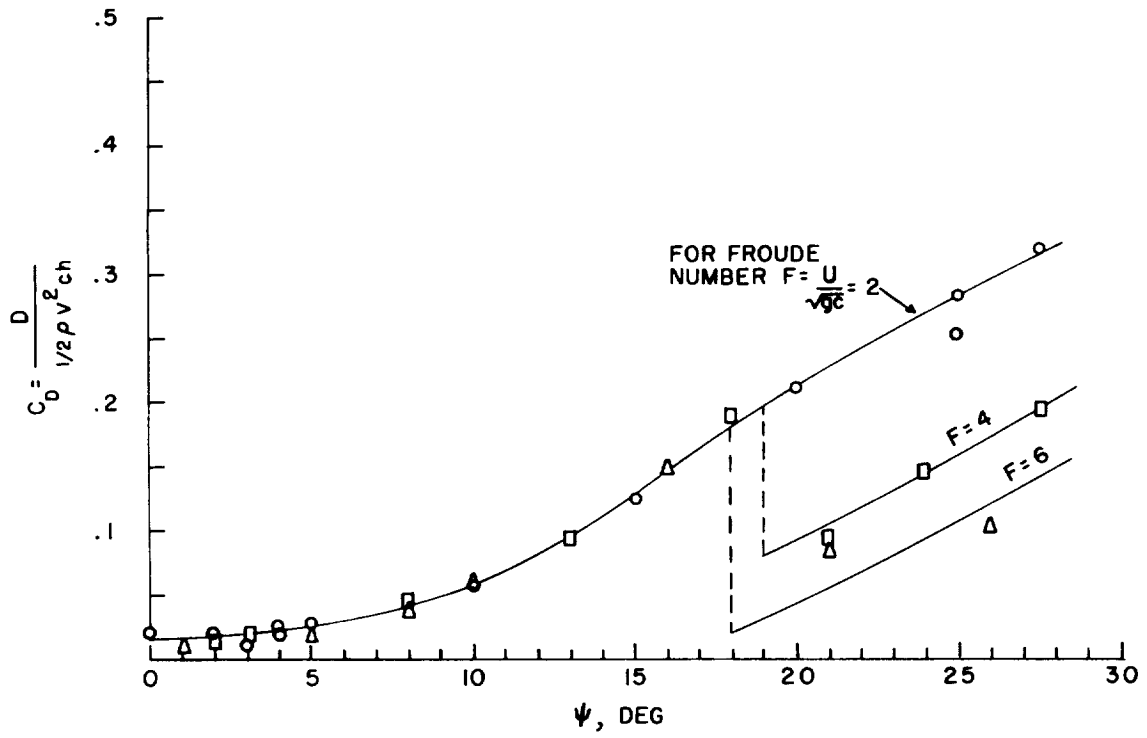
(c) Circular-arc strut; c = 2.5 inches; h = 5.0 inches; A = 2.0.

Figure 17.- Concluded.
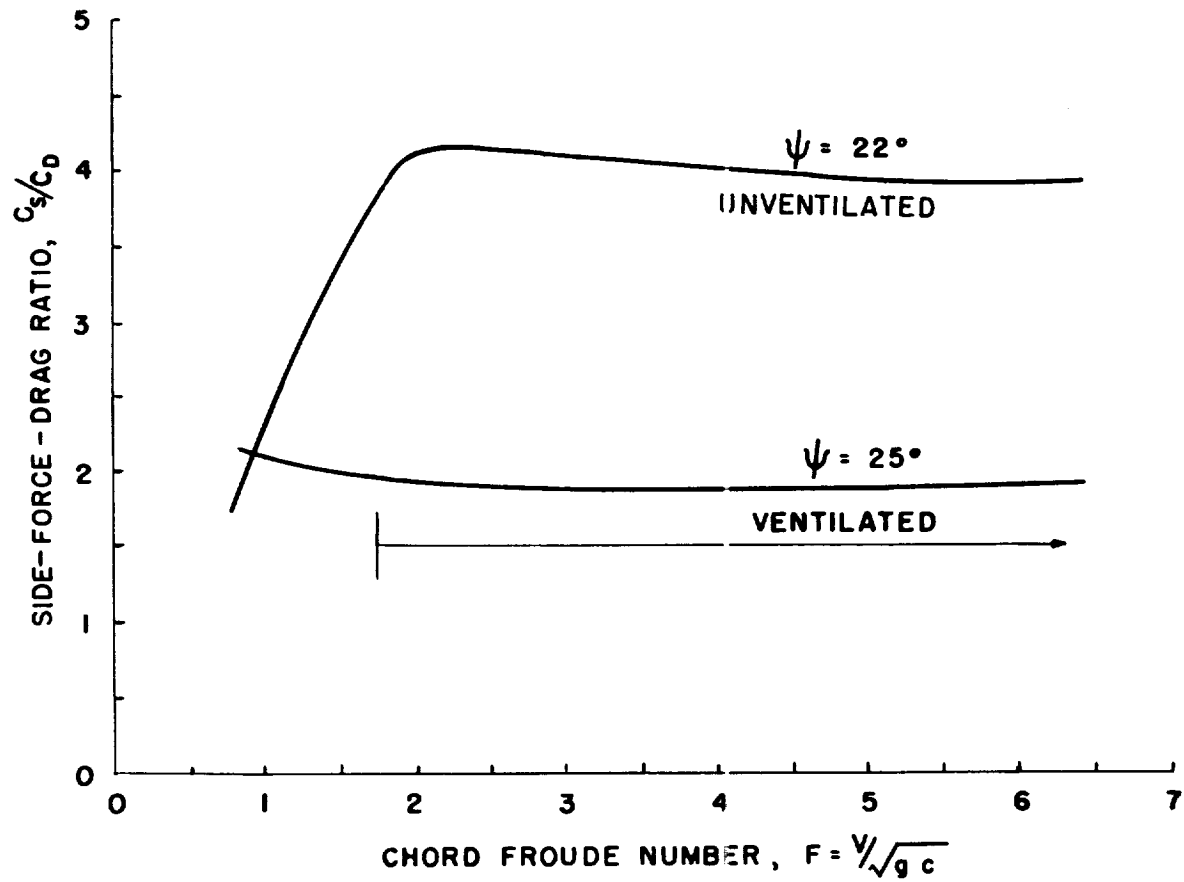
Figure 18.- Variation of side-force—drag ratio with Froude number with and without ventilation. NACA 4412 strut; A = 2.
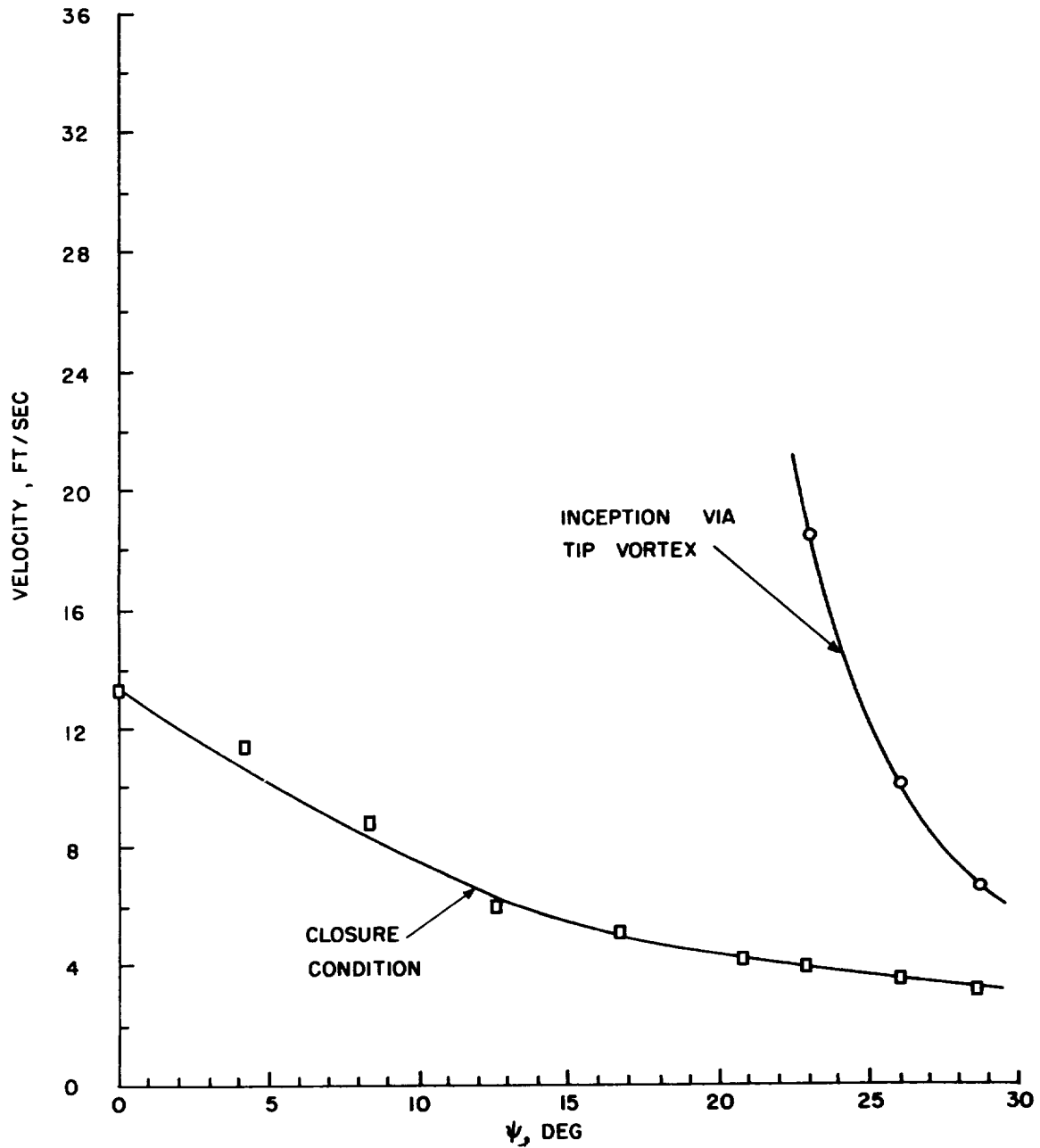
(a) NACA 4412 strut; c = 3.0 inches; h = 1.5 inches; A = 0.5.

Figure 19.- Velocity and angle of yaw at inception and closure of ventilated cavity.
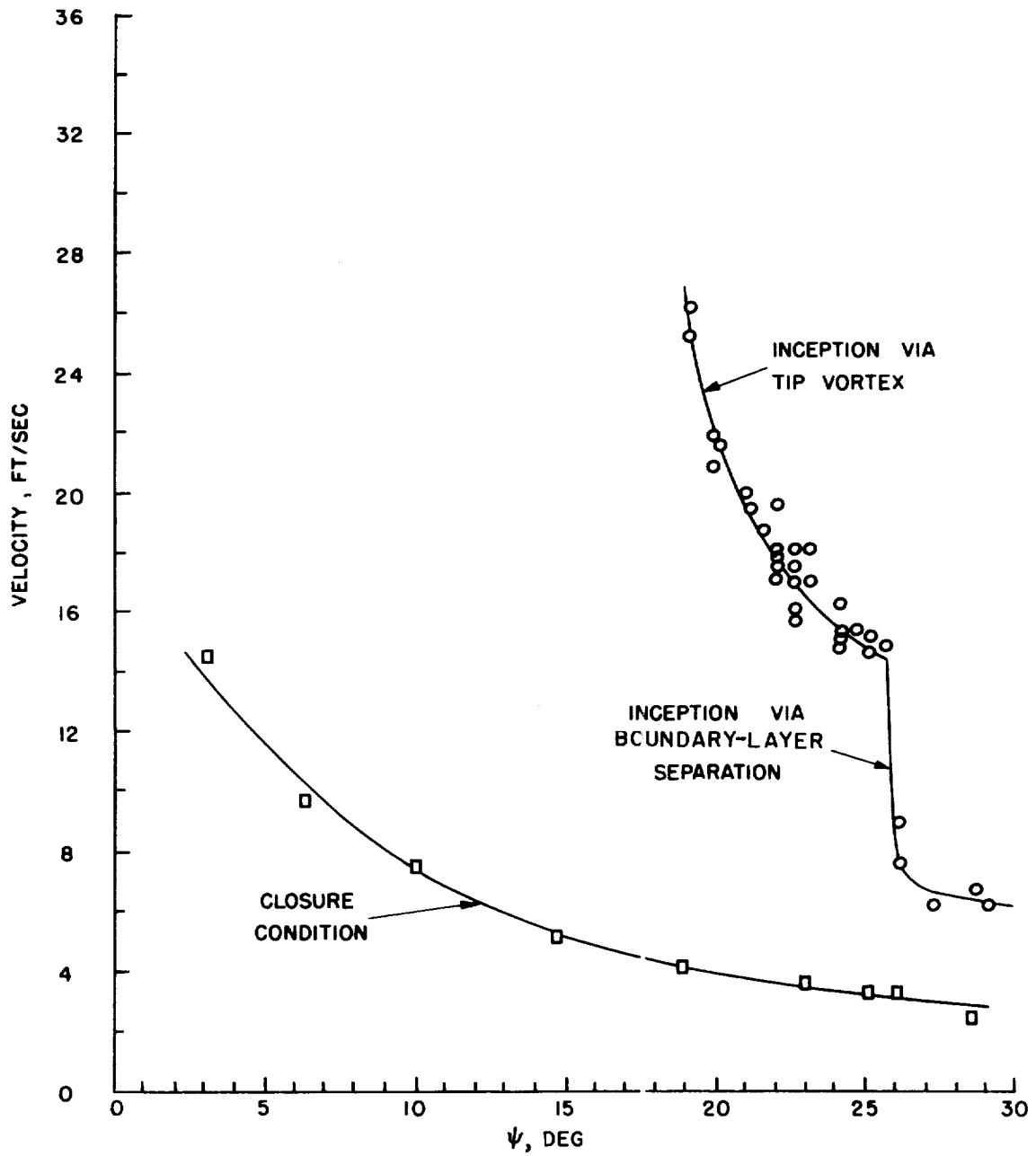
(b) NACA 4412 strut; c = 3.0 inches; h = 3.0 inches; A = 1.0.

Figure 19.- Continued.
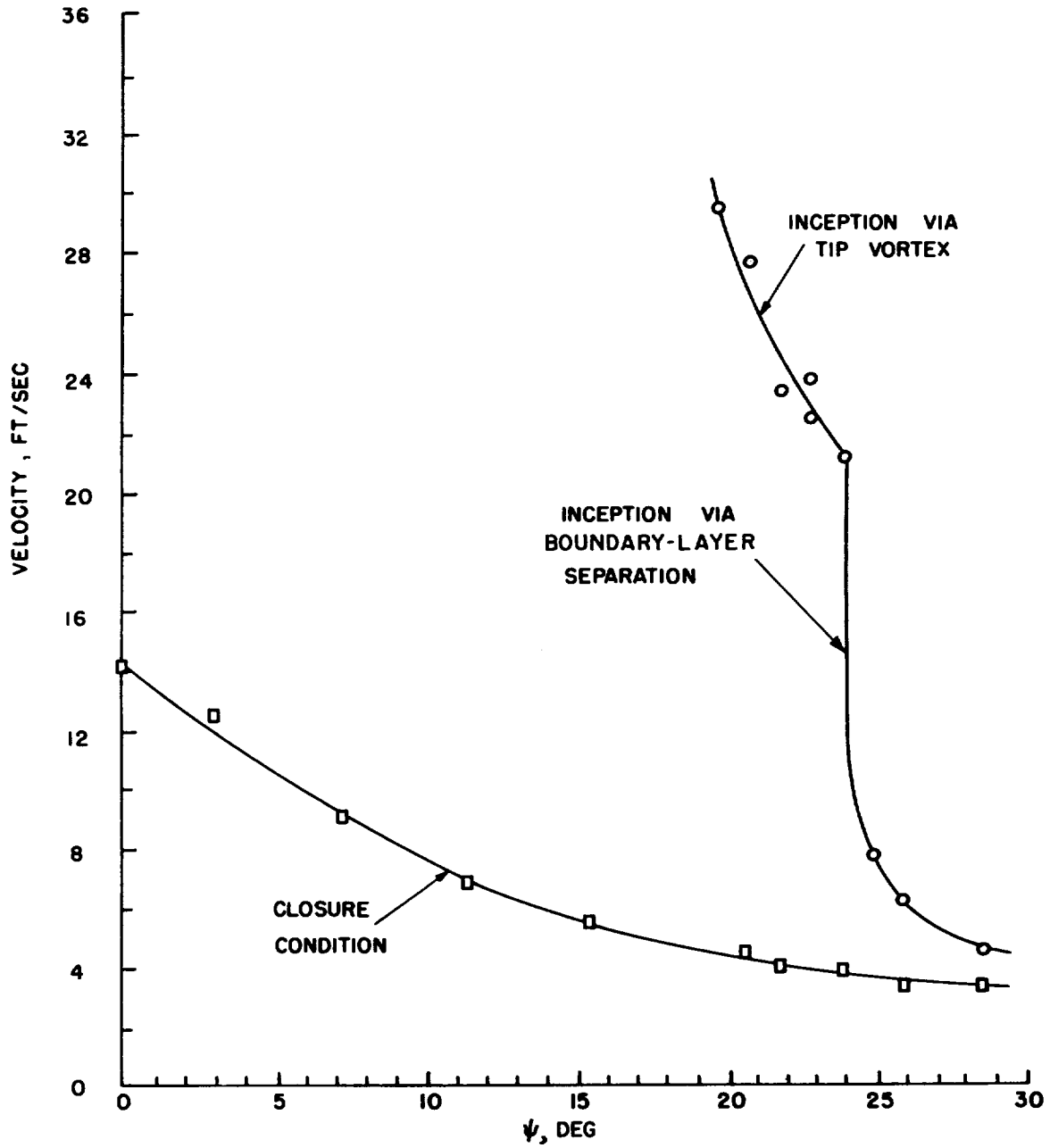
(c) NACA 4412 strut; c = 3.0 inches; h = 4.5 inches; A = 1.5.

Figure 19.- Continued.
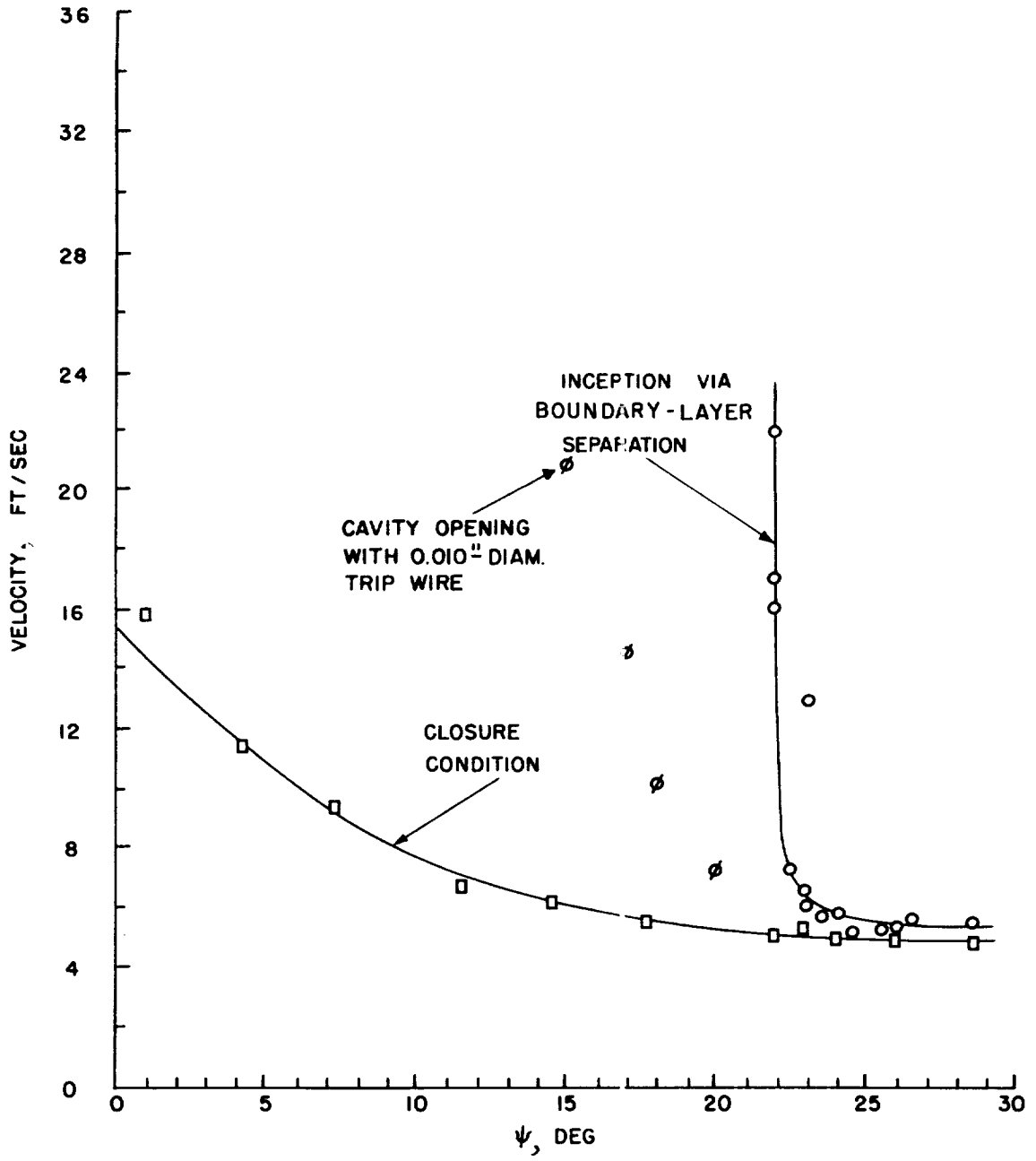
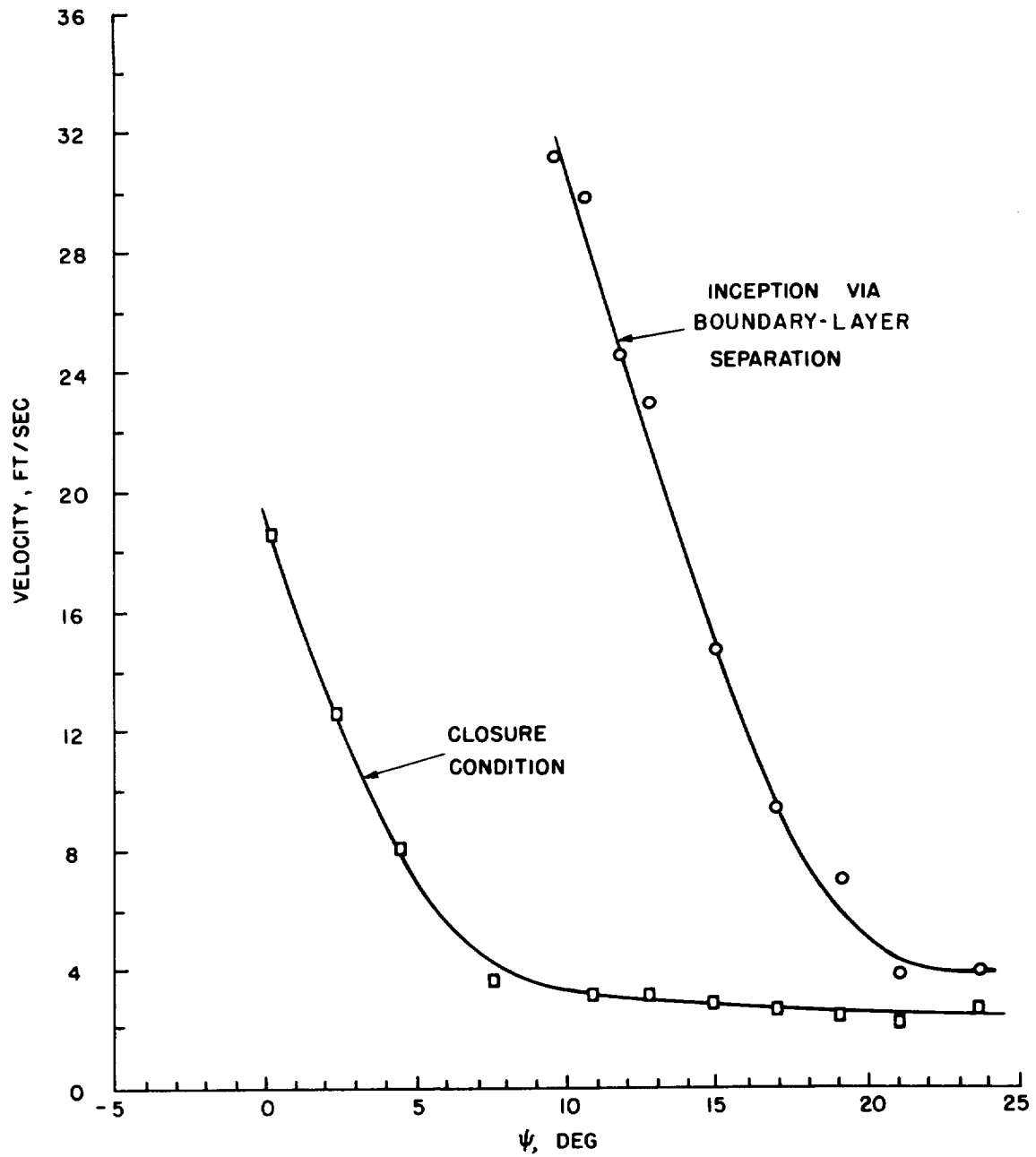(d) NACA 4412 strut; c = 3.0 inches; h = 6.0 inches; A = 2.

Figure 19.- Continued.
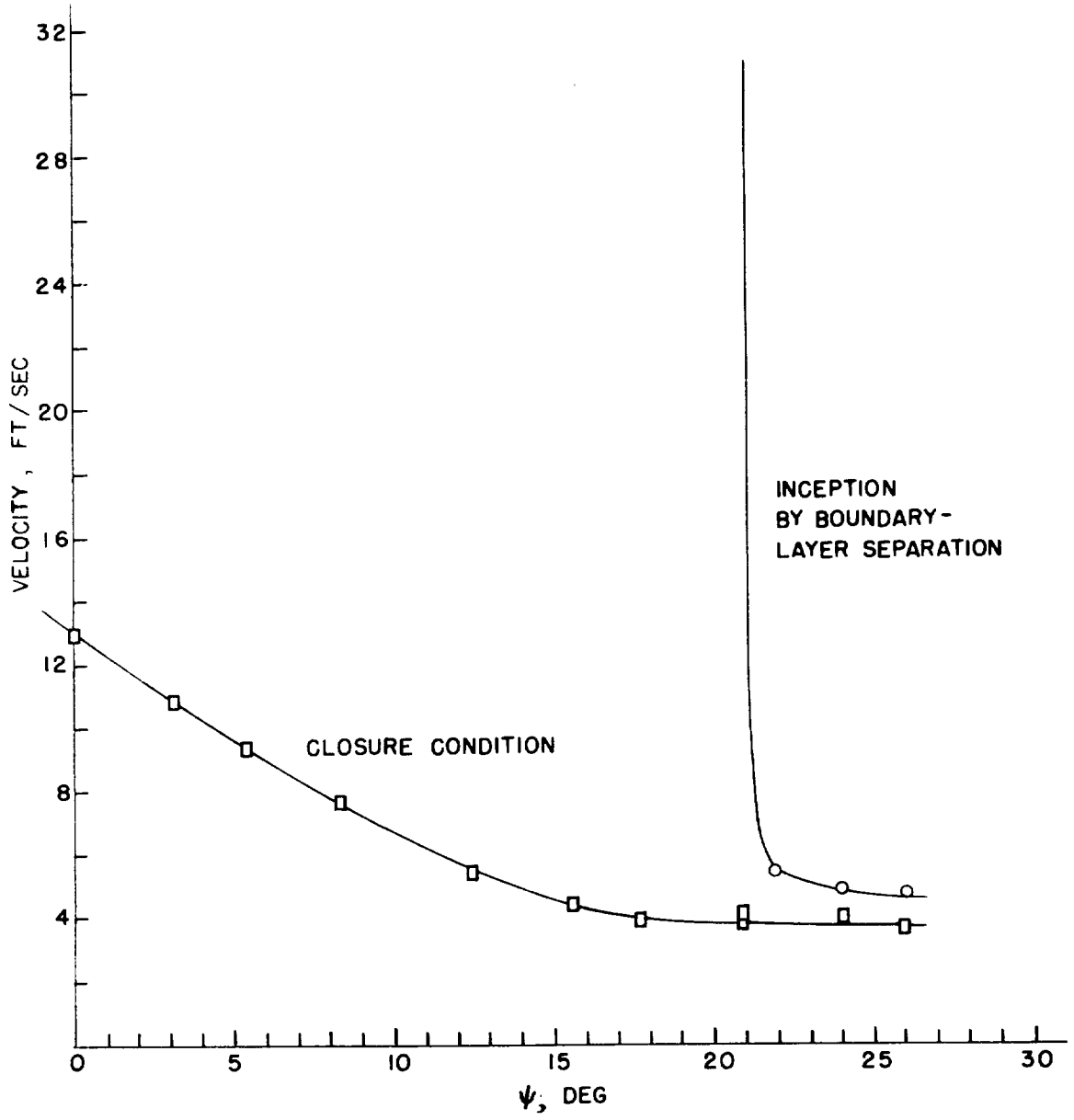
(e) NACA 4412 strut with 8-inch-diameter end plate; c = 3.0 inches; h = 3.0 inches; A = 1.0.

Figure 19.- Continued.
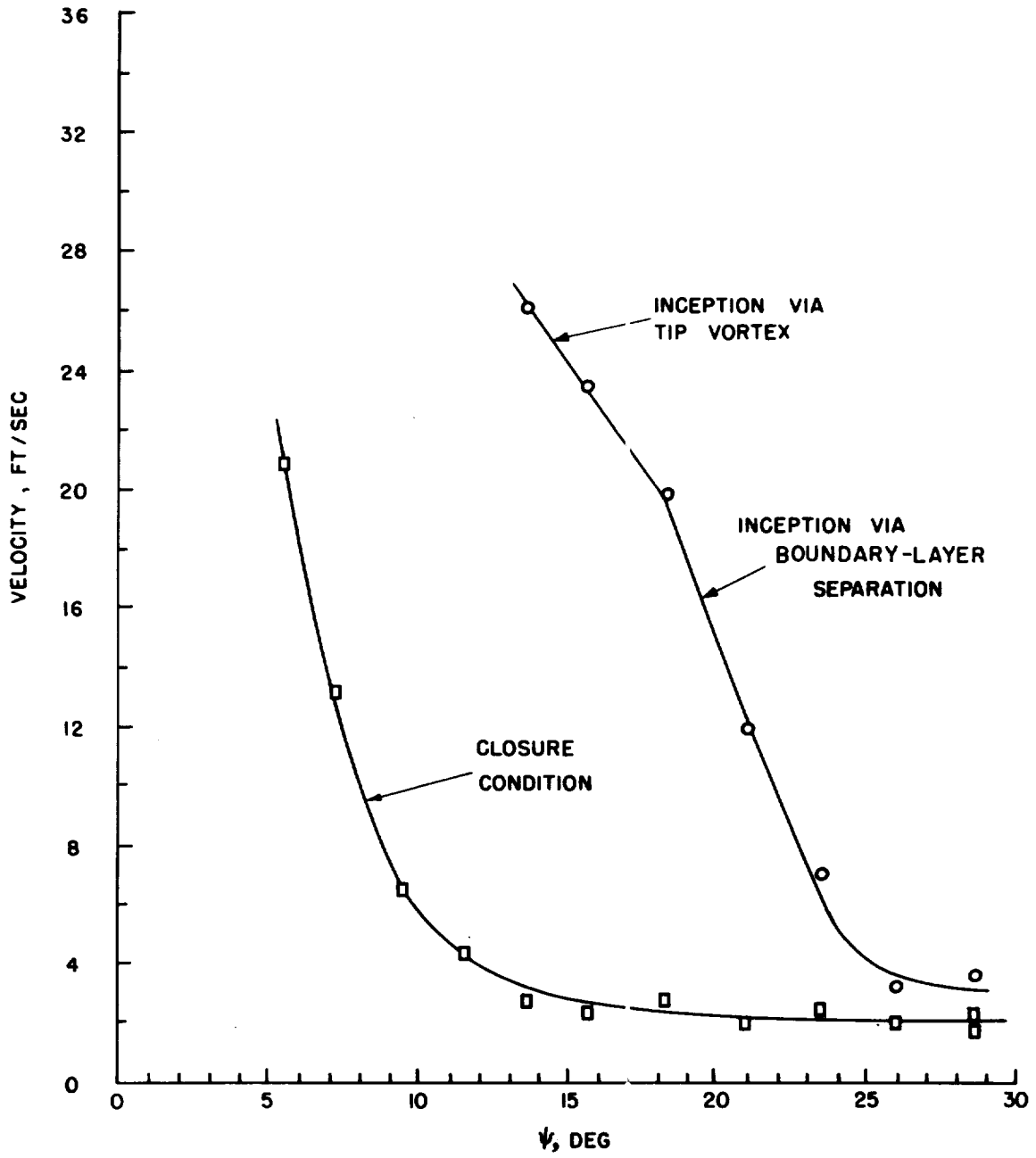
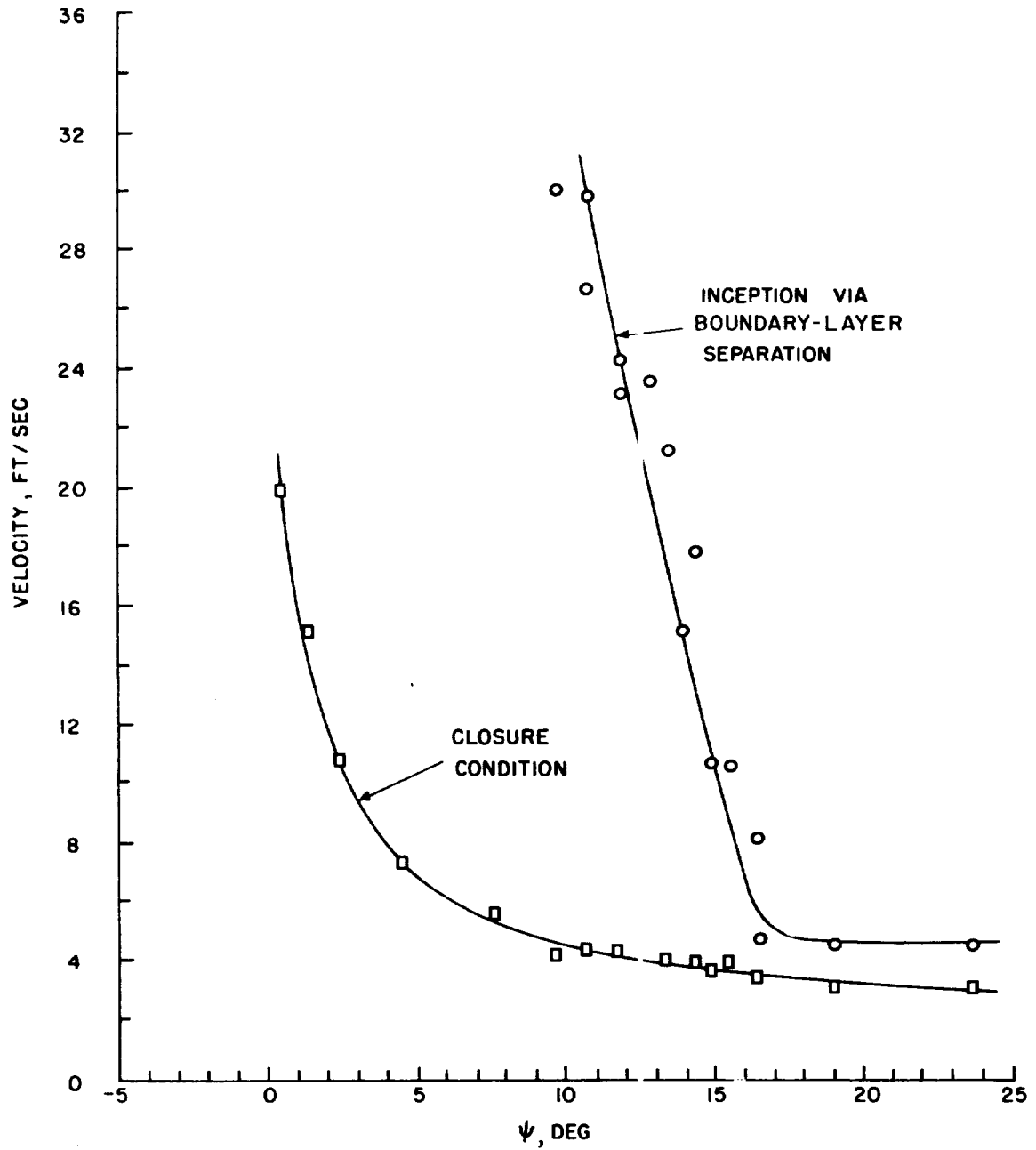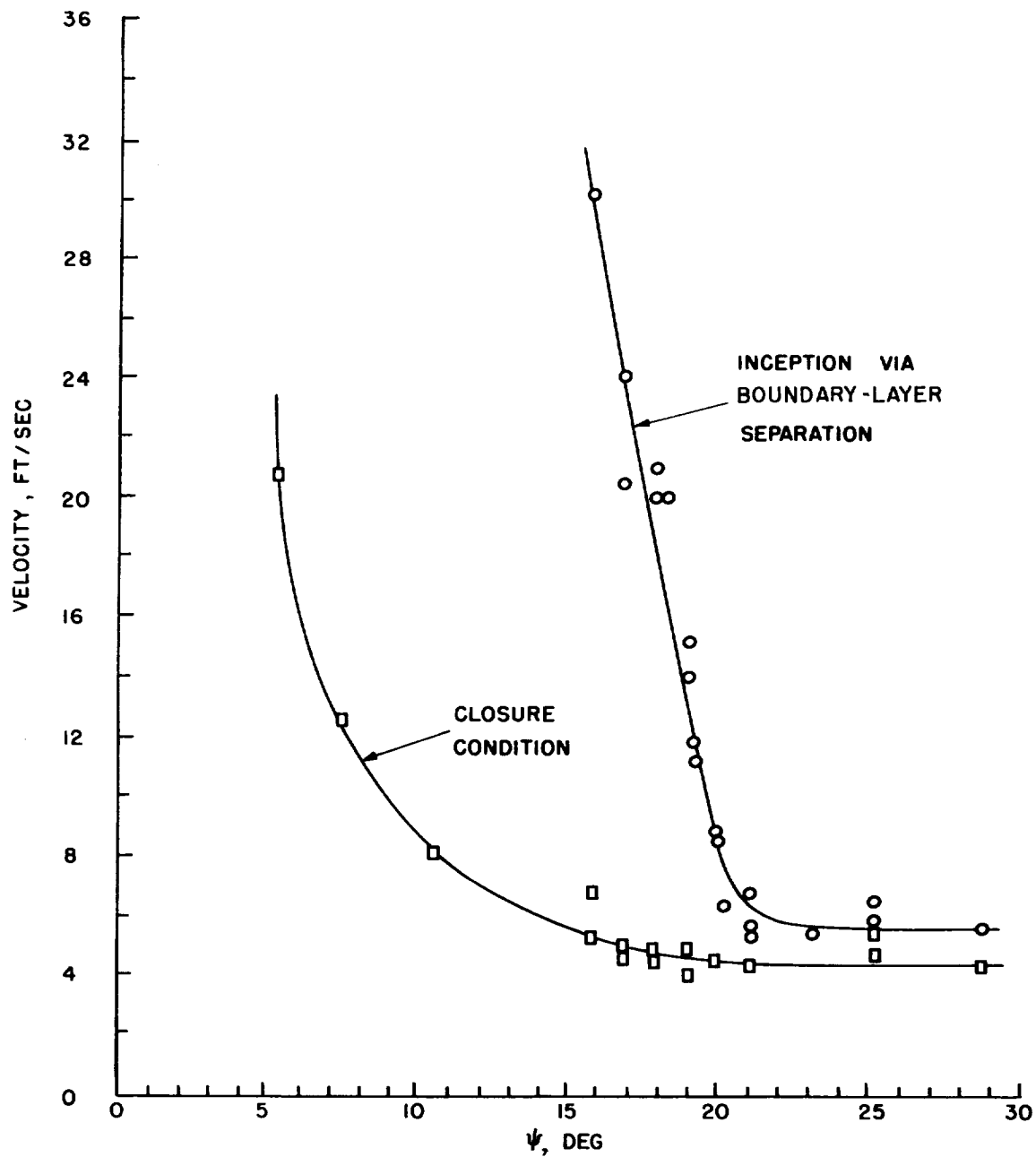(f) Circular-arc strut; c = 2.5 inches; h = 1.25 inches; A = 0.5.

Figure 19.- Continued.

(g) Circular-arc strut; c = 2.5 inches; h = 2.5 inches; A = 1.0.

Figure 19.- Continued.

(h) Circular-arc strut; c = 2.5 inches; h = 3.75 inches; A = 1.5.

Figure 19.- Continued.

(i) Circular-arc strut; c = 2.5 inches; h = 5.0 inches; A = 2.

Figure 19.- Concluded.

WITH TRIP WIRE WITHOUT TRIP WIRE

WATER
SURFACE

TRIP WIRE
(0.010" DIAM)

REGIONS OF
BOUNDARY—
LAYER
SEPARATION

SEPARATION WITH
REATTACHMENT
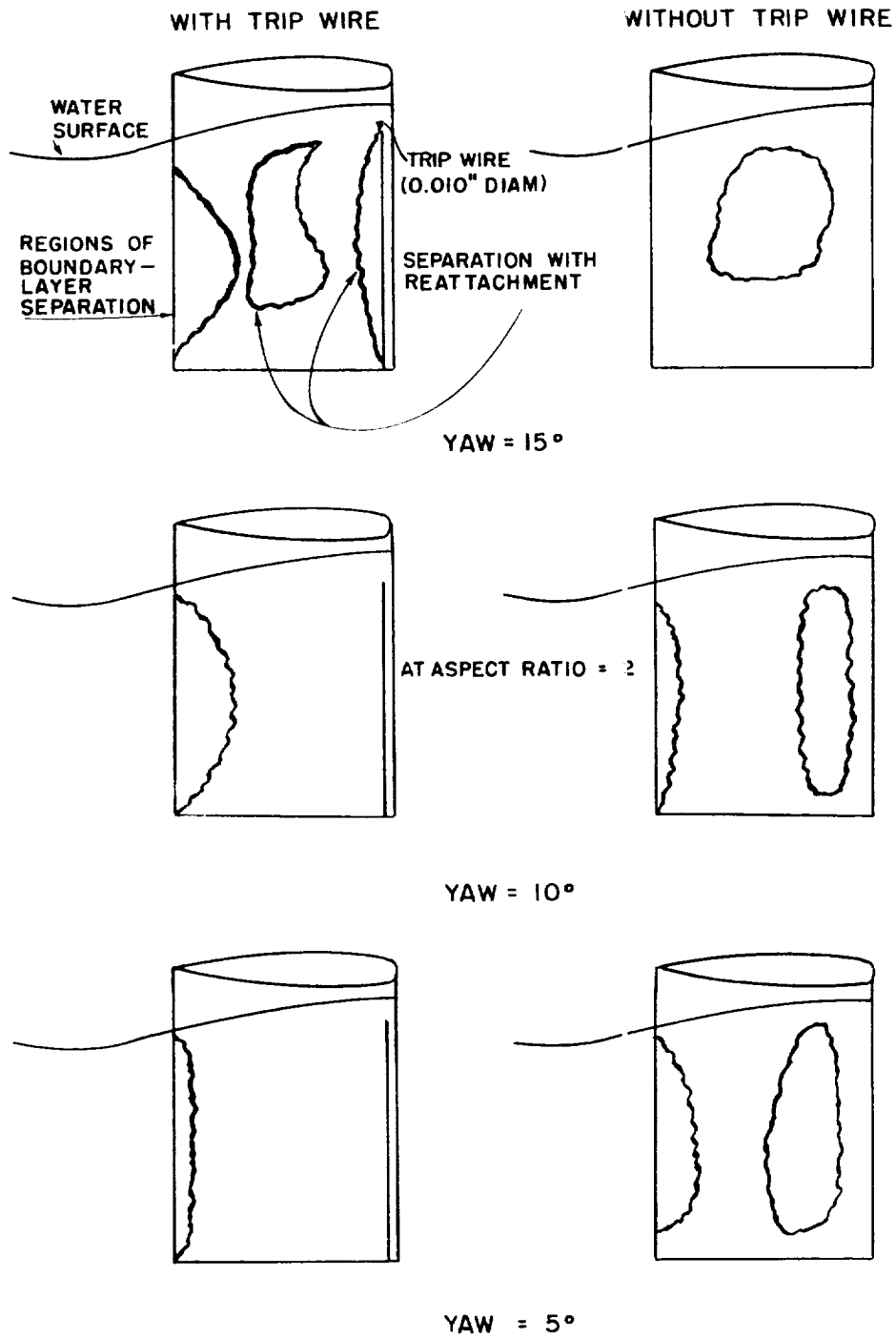
YAW = 15°

AT ASPECT RATIO = 2

YAW = 10°

YAW = 5°

Figure 22.- Regions of separation on NACA 4½-12 foil with and without
trip wire at Reynolds number $R = 3.4 \times 10^5$. Sketches are of suction
side.

WATER
SURFACE

HEAVY
SEPARATION

YAW = 10°

R = 0.95 x 10^5
(F = 2)

R = 2.9 x 10^5
(F = 6)

0.22 c

YAW = 15°

0.16 c

R = 0.95 x 10^5
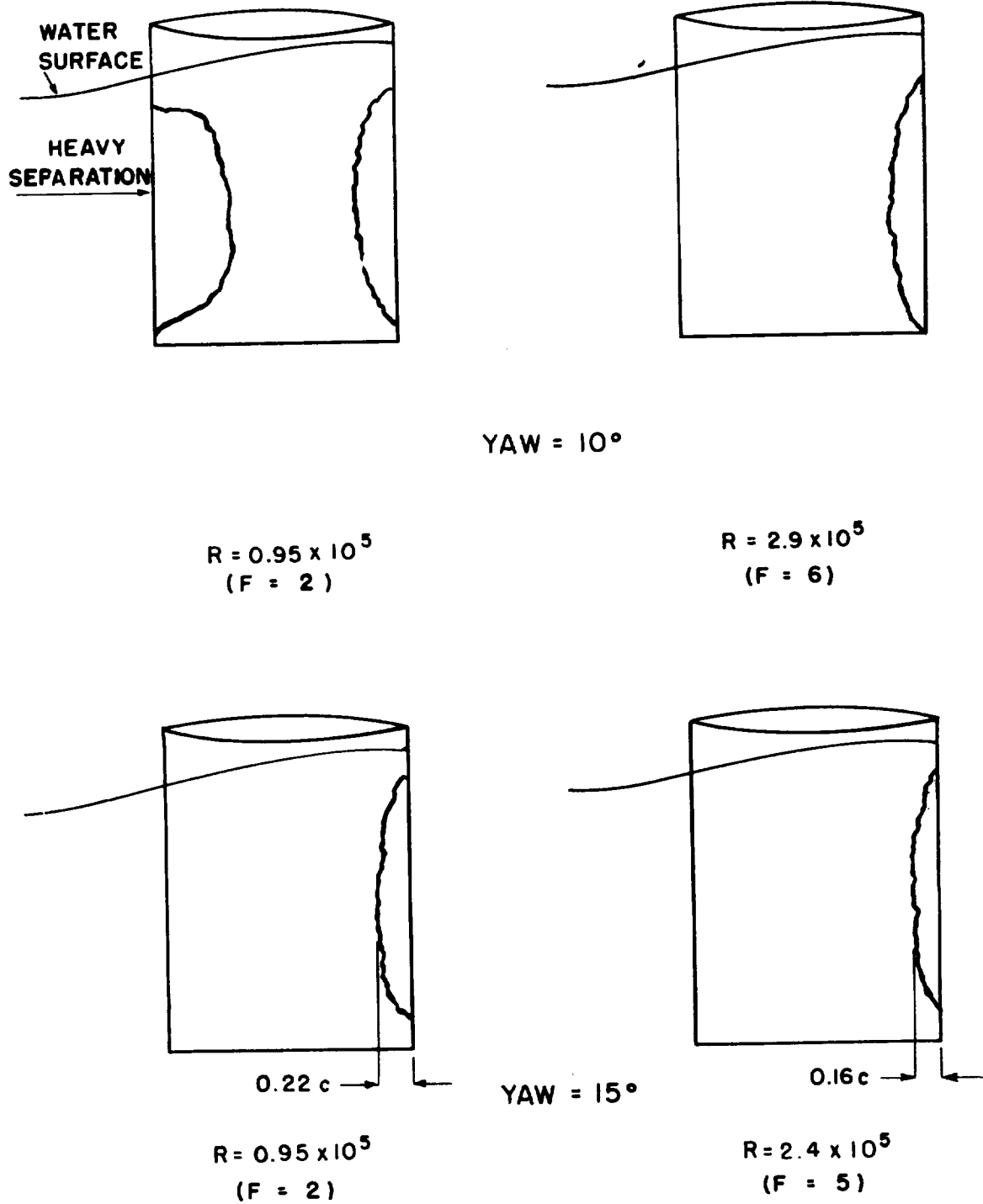(F = 2)

R = 2.4 x 10^5
(F = 5)

Figure 23.- Regions of separation on circular-arc strut without trip
wire. Sketches are of suction side.